Published in final edited form as:

Toxicol Pathol. 2016 June ; 44(4): 502–535. doi:10.1177/0192623316631844.

Proceedings of the 2015 National Toxicology Program Satellite Symposium

Susan A. Elmore[1], **Cindy A. Farman**[2], **James R. Hailey**[3], **Ramesh C. Kovi**[4], **David E. Malarkey**[1], **James P. Morrison**[5], **Jennifer Neel**[6], **Patricia A. Pesavento**[7], **Brian F. Porter**[8], **Kathleen A. Szabo**[5], **Leandro B. C. Teixeira**[9], and **Erin M. Quist**[1]

[1]National Toxicology Program, National Institute of Environmental Health Sciences, National Institutes of Health, Research Triangle Park, North Carolina

[2]Genentech, Inc., South San Francisco, California

[3]Covance Laboratories, Inc., Chantilly, Virginia

[4]Experimental Pathology Laboratories, Inc., Research Triangle Park, North Carolina

[5]Charles River Laboratories, Inc., Durham, North Carolina

[6]College of Veterinary Medicine, North Carolina State University, Raleigh, North Carolina

[7]School of Veterinary Medicine, University of California at Davis, Davis, California

[8]Texas A&M University, College Station, Texas

[9]University of Wisconsin-Madison, Madison, Wisconsin

Abstract

The 2015 annual National Toxicology Program (NTP) Satellite Symposium, entitled “Pathology Potpourri” was held in Minneapolis, Minnesota at the ACVP/ASVCP/STP combined meeting. The goal of this symposium is to present and discuss diagnostic pathology challenges or nomenclature issues. Because of the combined meeting, both laboratory and domestic animal cases were presented. This article presents summaries of the speakers’ talks, including challenging diagnostic cases or nomenclature issues that were presented, along with select images that were used for audience voting and discussion. Some lesions and topics covered during the symposium included hepatocellular lesions; a proposed harmonized diagnostic approach to rat cardiomyopathy; crop milk in a bird; avian feeding accoutrement; heat exchanger in a tuna; metastasis of a tobacco carcinogen-induced pulmonary carcinoma; neurocytoma in a rat; pituicytoma in a rat; rodent mammary gland whole mounts; dog and rat alveolar macrophage ultrastructure; dog and rat pulmonary phospholipidosis; alveolar macrophage aggregation in a dog; degenerating yeast in a cat liver aspirate; myeloid leukemia in lymph node aspirates from a dog; *Trypanosoma cruzi* in a dog; solanum toxicity in a cow; bovine astrovirus; malignant microglial tumor; and nomenclature

Address correspondence to: Susan A. Elmore, National Toxicology Program, Cellular and Molecular Pathology Branch, National Institute of Environmental Health Sciences, National Institutes of Health, Research Triangle Park, NC 27709, USA; elmore@niehs.nih.gov.

The author(s) declared no potential conflicts of interest with respect to the research, authorship, and/or publication of this article.

The author(s) received no financial support for the research, authorship, and/or publication of this article.

challenges from the Special Senses International Harmonization of Nomenclature and Diagnostic Criteria (INHAND) organ working group (OWG).

Keywords

NTP Satellite Symposium; cardiomyopathy; pulmonary ultrastructure; crop milk; oral ornamentation; tuna heat exchanger; histoplasmosis; leukemia +/− cytology; mammary gland whole mounts; diagnostic neuropathology; ocular inflammation; INHAND; neurocytoma; persistent fetal vasculature; persistent hyperplastic primary vitreous; persistent hyperplastic tunica vasculosa lentis; focal nodular hyperplasia; pulmonary metastatic tumor

INTRODUCTION

The NTP Satellite Symposium is a one-day meeting that is traditionally held in conjunction with the annual Society of Toxicologic Pathology (STP) meeting (Adams *et al.* 2011; Bach *et al.* 2010; Boorman *et al.* 2012; Elmore *et al.* 2013; Elmore *et al.* 2014; Elmore *et al.* 2015). This year the meeting was held at the first combined meetings of the STP, American College of Veterinary Pathologists (ACVP) and American Society for Veterinary Clinical Pathology (ASVCP). The objective of this annual symposium is to provide continuing education on interpreting histopathology slides. This includes the presentation and discussion of diagnostically difficult, interesting, or rare lesions, or challenging nomenclature issues. The session is interactive in that each speaker presents images for audience voting via wireless keypads. Once the votes are tallied the results are displayed for all to view. The speaker generally provides a preferred diagnosis and some additional background information, after which lively and constructive discussion ensues.

The theme for the 2015 Symposium was “Pathology Potpourri,” which allowed for a variety of topics to be presented. The format for this year’s symposium included a mixture of laboratory, wildlife and domestic animal cases featuring a wide variety of species that included rat, dog, cat, bird, fish, cow and rabbit. Tissues included liver, heart, crop, feeding accoutrement, heat exchanger, pancreas, pituitary gland, mammary gland, lung, spinal cord and brain. Also presented were liver and lymph node aspirates. Finally, two speakers presented diagnostic challenges from the ocular system that were being considered by the Special Senses INHAND OWG. This article provides synopses of all presentations including the diagnostic or nomenclature issues, a selection of images presented for voting and discussion, voting choices, voting results, and major discussion points.

IT’S NOT A TUMOR?

Dr. Dave Malarkey of the National Institute of Environmental Health Sciences and National Toxicology Program (NIEHS, NTP, Research Triangle Park, NC) presented the first two cases of the day. He presented two lesions that challenged the dogma regarding the occurrence and fate of benign nodular lesions of hepatocytes in the rodent and dog. To further emphasize the comparative nature of these cases for this combined meeting, related lesions in humans were also discussed.

The first case (Courtesy of Marshfield Labs, Marshfield, WI) was a biopsy of an exophytic, expansile, 2-cm diameter mass on the diaphragmatic surface of the left lateral liver lobe in a 12-year-old spayed female dachshund (Figure 1A). The dog presented with recurrent cystic calculi, cardiomyopathy, hepatomegaly, and mildly elevated liver enzymes. Histologically, the mass was comprised of well-differentiated hepatocytes forming single- to double-walled plates with expanded lobules and scattered portal tracts throughout. Minimal portal bridging inflammation, fibrosis, and biliary hyperplasia accentuated the lobular architecture (Figure 1B).

The majority of audience members voted that the mass was either focal nodular hyperplasia of hepatocytes (30%) or a diaphragmatic hernia entrapping part of the liver lobe (61%). A few people voted for hepatocellular neoplasm (9%). Nodular hyperplasia of hepatocytes is a frequent incidental finding in the dog and can be found at any age. It is one of the most common lesions in the dog liver and is grossly and clinically indistinguishable from hepatocellular neoplasms. In contrast to nodular hyperplasia, diaphragmatic hernia of the liver is an uncommon lesion in the dog. A quick poll of the audience showed that about 15% (or 30 pathologists) have observed a diaphragmatic hernia of the liver in the dog. An incidence ranging from 1 to 11% has been reported for hepatodiaphragmatic nodules in Fischer 344 rats (Eustis et al., 1990) with few cases reported in other rat stocks and strains. Mice do not develop such nodules, but may have focal lesions similar to those in rat. Hepatodiaphragmatic nodules can be seen in rats at any age and their occurrence in fetuses is considered presumptive evidence of a congenital origin. While they appear protrude through the diaphragm and extending into the thoracic cavity, they actually are attached to and covered by a thin fibrous portion of the diaphragm (Eustis et al., 1990). Histologically, the liver maintains lobular structure, although distorted.

For comparison, an example of focal nodular hyperplasia (FNH) was presented, (courtesy of Dr. Gordon Flake of NIEHS) and discussed. Histologically, FNHs frequently have portal bridging fibrosis and inflammation with biliary hyperplasia (Bosman et al., 2010). It is proposed to be a regenerative nodule secondary to localized vascular abnormalities with increased blood flow. FNH has also been shown in women to be related to exogenous hormone administration, such as oral contraceptives. Such nodules regress after cessation of the exogenous hormones.

After reviewing the characteristics of FNH, a revote for this first case showed that the audience still favored a diagnosis of “diaphragmatic nodule” (62%). 19% voted for nodular hyperplasia of hepatocytes, 12% voted for hepatocellular carcinoma and 6% voted for focus of altered hepatocytes.

The second case was that of a 15-year-old castrated male golden retriever (courtesy of Dr. John Cullen of North Carolina State University). The favored diagnosis was hepatocellular adenoma (59%) and fewer favored hepatocellular carcinoma (18%), hepatocellular nodular hyperplasia (15%), focus of altered hepatocytes (6%), cirrhosis (1%) and “other” (1%). A year earlier this dog was diagnosed with hepatic hemangiosarcoma by cytology after a liver mass was detected by ultrasound. Histologically, the mass was well-circumscribed, expansile, and comprised of haphazardly arranged well-differentiated hepatocytes with no

apparent lobular structure, and forming trabeculae two cells thick in some areas. For years hepatocellular adenoma was not recognized as an appropriate diagnosis in the dog. Rather, these types of lesions were considered either nodular hyperplasia or well-differentiated hepatocellular carcinoma. The prognosis for adenoma is good, however malignant transformation can occur. By comparison, hepatocellular adenoma is rare in people (3/100,000) and 85% of these occur in young women. The risk factors include exposure to estrogenic and androgenic steroids, obesity, glycogenoses, galactosemia, and iron-overload. Again, most regress after the cessation of exogenous hormones.

After the discussion, a revote demonstrated that the majority still favored hepatocellular adenoma (65%) and fewer favored hepatocellular carcinoma (15%), hepatocellular nodular hyperplasia (7%) or focus of altered hepatocytes (13%).

CARDIOMYOPATHY SHUFFLE

Dr. James (Rick) Hailey (Covance Inc., Chantilly, VA) presented 6 cases of varying morphological presentations of a single disease entity, cardiomyopathy, in young Sprague Dawley (SD) rats up to 15 weeks of age. These cases were selected to assess differences in terminology, thresholds for diagnosis of small lesions, and thresholds for severity categorization used by the audience. Because this was a combined meeting with the ACVP the audience consisted of pathologists with varying levels of experience with these types of lesions. Some of the lower magnification images provided to the audience are not included in this summary of the proceedings.

To assess potential differences in diagnostic terminology used by the audience, and to challenge one’s ability to consistently apply multiple diagnostic terms to the spectrum of lesions known to comprise “cardiomyopathy”, these cases included representations of the range, and/or combination of morphologies. The morphology for case 1 was primarily necrosis (Figure 2A), case 2 was primarily cellular (Figures 2B and 2C), case 3 was a mixture of necrosis and cellular infiltration (Figures 2D, 2E and 2F), and case 4 was high magnification of four small lesions with varying morphologies within the same heart (Figures 2G, 2H, 2I & 2J). Voting choices included (1) inflammatory cell infiltrate, (2) necrosis, (3) fibrosis, (4) 1 & 2 (this represents two separate diagnoses as opposed to option 8 which is a single diagnosis), (5) 1 & 3, (6) 1, 2 & 3, (7) degeneration/necrosis, (8) necrosis/inflammatory cell infiltrate (NICI) and (9) cardiomyopathy.

To assess the use of thresholds for diagnosing cardiomyopathy, case 5 was a morphology that could be interpreted as cardiomyopathy with some level of uncertainty (Figure 2K), and case 6 was a clear cardiomyopathy (Figures 2L), but a tiny lesion. The voting choices for these two cases were similar to the first four cases except the choices for 5) 1 & 3 and 6) 1, 2 & 3 were removed and replaced with voting options that included “not a lesion or equivocal” and “a definite lesion, but below my threshold for routinely diagnosing”.

To assess potential variability in assignment of severity grades, case numbers 2 and 3 were presented to represent mild severity that was only slightly above the threshold for minimal severity. Case 4 was presented to represent minimal severity despite the multiplicity of the

lesions, as the aggregate lesion size was less than that of single lesions in each of cases 3 and 4. These grades were established based upon the voting preferences of pathologists voting in previous exercises (to be published). Voting options for severity included (1) minimal, (2) mild, (3) moderate, and (4) severe. The audience was told prior to voting that the hearts were from both control or treated rats, that all lesions in case 4 were from the same heart, and that the location of lesions within the heart should not impact their diagnoses.

Voting results are summarized in Table 1. Consistent with intrinsic differences as well as differences in experience and training, there was diversity of diagnostic approach among the audience with no less than 6 voting options receiving votes in all 6 cases with votes representing all 9 choices for case 1. Overall, single or combined (slash) terms were preferred. Votes for case 1, which was predominately necrotic, were fairly evenly split between degeneration/necrosis, NICI and cardiomyopathy. Inflammatory cell infiltrate garnered the most votes for cases 2 and 6, which were predominately cellular. NICI and cardiomyopathy both capture a spectrum of morphological change and received the most votes for cases 3 and 4 which were comprised of a somewhat equal mix of necrosis and cellular infiltrate.

Most of the audience did not use a threshold for diagnosing tiny but clear lesions as case 6 was diagnosed as inflammatory cell infiltrate by 42% of the participants. However, 30% of the audience did use a threshold as they did not diagnose it despite considering it a lesion, and fewer (14%) considered it equivocal or not a lesion. Case 5 was included as a morphology that potentially represented cardiomyopathy, but was not definitive (e.g. also could represent the edge of a vessel). While “equivocal” received 44% of the votes, 56% considered it a lesion, although some considered it below their threshold for diagnosing.

Severity grades were requested for cases 2, 3 and 4, and votes were split. Minimal and mild clearly garnered the most votes, however, there were up to 19% of votes for moderate severity and up to 6% of votes for the highest severity grade option. Multiplicity may affect assignment of severity score of mild as that was mentioned as a factor during the discussion of these cases. Also, case 4, which contained 4 lesions with aggregate size less than the size of the single lesions in each of cases 2 and 3, received the most number of votes for mild or greater severity. The audience’s perspective for severity grading was limited by the number of images shown and lack of relative comparisons.

Histopathological examination of the heart in rodent toxicity studies is an important endpoint in assessing potential risk of cardiotoxicity in patients. The presence of spontaneous murine cardiomyopathy in the SD rat and other rat strains may confound identification and/or interpretation of potential test article (TA)-related cardiotoxicity as the incidence and morphologic appearance is often variable, and the spontaneous lesion may overlap in morphology with that directly caused by or associated with drug effects either via exacerbation of cardiomyopathy or a separate mechanism (Greaves, 2000; Jokinen et al, 2011). Consistency in the application of diagnostic term(s), and thresholds for diagnosing and assigning severity grades for cardiomyopathy/like lesions within a study is necessary to identify and interpret TA-related findings in the heart. Due to differences in training and/or

experiences, pathologists may have different diagnostic terms and thresholds for these lesions.

As evidenced by the voting, different diagnostic terminology was used by different pathologists for the same lesion. The majority used a combined (e.g. NICI) or single term (cardiomyopathy) to capture the spectrum of morphologies of this disease entity. However, some used multiple diagnoses for lesions of varying morphology (e.g. necrosis and inflammatory cell infiltrate). The spectrum of morphologies for these lesions in control animals is broad, as seen in these examples (necrosis → inflammatory cell infiltrate → fibrosis). Some (30%) used a threshold and therefore did not diagnose the smallest of lesions (case 6) while others diagnosed morphologies (case 5) that most would consider as uncertain, or not a lesion. The split in severity grades for cases 2, 3 and 4 demonstrate different thresholds for severity categorization of cardiomyopathy lesions among the audience participants.

Historical control data can be valuable for contextualizing study data. Historical data may be negatively impacted by varied diagnostic terminology, which makes mining and communicating historical control data problematic, and differing thresholds for diagnosis of lesions obviously negatively impacts historical control data. There are many “acceptable” approaches to diagnosing these lesions, and toxicologic pathologists must have latitude to approach a study in a manner that most appropriately accounts for, and communicates, TA-related effects. Consistency within a study by the pathologist is critical. However, in most instances, diagnosing the same lesion the same way by all pathologists offers the potential for a more robust historical control database, and may add a degree of precision that could result in more accurate study outcomes/interpretations.

A yet to be published potential “harmonized” diagnostic approach was presented to the audience suggesting use of (1) a single “slash” term [NICI, Chanut et. al., 2013], (2) use of no threshold for diagnosing lesions that clearly represent cardiomyopathy, no matter how small, and (3) use of ~1/2 the field of view using the 40X objective and 10X eyepiece as the criterion for separating minimal from mild severity grades. The audience was asked to discuss the pros and cons of using a harmonized diagnostic approach and the pros and cons of the various aspects of the specific diagnostic approach presented.

There was consensus about the need for good historical control data; however, getting reliable data is the challenge. Relative to diagnostic terms, some consider it best to initially use multiple terms to more accurately capture the varying morphologies. After evaluating the data, if there are no “signals”, one can then consolidate the terminology. If something different or unexpected is observed with the multiple terms, they are retained. Some consider a slash term to be confusing; does NICI imply “necrosis and inflammation” or “necrosis or inflammation”? The slash term may indicate to some that you cannot really figure out which lesion is present. To others it would indicate that both lesions are present. One participant opined that use of a slash term is acceptable if both components are part of the same lesion, but not to represent multiple lesions. Charlotte Keenan, current chair of INHAND Global Editorial Steering Committee and ad-hoc member of the SEND Controlled Terminology Committee, commented that SEND is prepared to accept slash terms such as ‘degeneration/

regeneration' if the individual terms are present in the controlled terminology list and the combination represents a spectrum of either lesion. One participant was concerned that NICI may not work well for longer-term studies with older animals having greater amounts of fibrosis. It was suggested that cardiomyopathy might be a better single term to capture the spectrum of lesions, as it would cover the progression of the lesion as the animal ages. Other terms and/or combinations of terms have their limitations, and although not perfect, NICI received more votes than cardiomyopathy for these lesions in young animals by this audience.

Commonality is important when companies use different contract laboratories to read studies; therefore, a harmonized diagnostic approach could be helpful. Relative to severity grading, there was a suggestion that size and number are important for severity grading. Because of previous published reports, it was queried whether there is predilection for any specific sites within the heart. Chanut and colleagues (2013) showed that all parts of the heart may be affected and that lesions tend to be random, however, that study was not designed to definitively answer the question of site predilection. Lesions in the cases presented by Dr. Hailey were from various regions of the heart including the left and right ventricles, septum, base and apex of the heart. However, these lesions were only selected to demonstrate the lesion of cardiomyopathy and not the varied locales or randomness of cardiomyopathy within the heart. One participant highlighted the importance of assessing adversity and/or human relevance with regard to cardiomyopathy/like lesions.

In summary, it was clear that approaches for diagnosing these lesions is quite variable between pathologists. There was consensus that a more harmonized diagnostic approach, particularly with regard to use of thresholds, could enhance historical control data. Audience participants were split on the best diagnostic terminology to use, and discussion time was too limited to gain consensus on terminology or thresholds for diagnosing and severity grading of cardiomyopathy-like lesions.

QUERIES FROM THE ZOO

Dr. Patricia Pesavento (School of Veterinary Medicine, UC Davis, CA) chose histologic oddities that are normal physiologic variations of a variety of animals. Her first case was tissue from a rock dove (pigeon). After review of Figures 3A and 3B, including higher magnifications, the audience was asked to vote on the etiology. The choices and voting results were vitamin A deficiency (27%), poxvirus (19%), normal (18%), "I don't know" (12%), *Trichomonas* (9%), *Candida* (8%), zinc deficiency (6%) and trauma (1%). The majority of audience members had most likely never seen this tissue before so most of the votes were clearly guesses. The most honest votes were probably for "I don't know"!

This unusual tissue presentation was that of "crop milk", which is associated with remarkable epithelial hyperplasia in the lower esophagus/crop of a pigeon (Dumont, 1965). Figure 3A shows a transition from non-glandular crop with a thin epithelial lining to a deeply hyperplastic, convoluted epithelial layer. The epithelial/subepithelial junction, normally quite flat, is thrown into deep folds with a congested capillary bed nested among the interlacing islands/nests of basilar epithelium (Figure 3C).

The young of a small subset of birds are fed these special secretions called “crop milk”. The crop milk is produced by the sloughing of fat and protein laden epithelial cells (Figure 3D) from a hyperplastic lining of the crop, which is normally a thin-walled non-glandular food storage chamber at the base of the esophagus. The evolutionary strategy of using crop milk has not developed in all birds, but among those where crop milk is used, pigeons, doves, penguins, and flamingos are the best studied. Table 2 shows the percent composition of milk from various avian and mammalian species. Like mammalian milk, crop milk is extremely nutritious, and contains immunoglobulin (IgA) (Ricarda et al. 1992; Tizard, 2002). In one study, domestic chicks given feed containing pigeon crop milk were 16 percent heavier at the end of the experiment than chicks that did not receive the crop milk supplement, and in a 1952 study where pigeon crop milk was fed to chickens, their rate of growth improved by 38% (Pace et al. 1952; Hegde 1972). Chickens fed with pigeon crop milk had a different microbial composition in their caeca compared to control chickens, and they showed significant enrichment of immune-related genes among the genes differentially expressed in GALT tissues (Gillespie et al. 2011; Gillespie et al. 2013). Crop milk contains much more protein (and fat) than cow milk (30% vs. 3–5%). It is the exclusive food of the pigeon and dove nestlings for several days after hatching, and apparently the exclusive nutrition for over two months of greater flamingo nestlings. It is difficult to find references that include histology, but flamingo milk is not produced exclusively in the crop and involves glands lining the entire upper digestive tract. Greater flamingos’ milk reportedly contains an abundance of red and white blood cells, which are also reportedly mobile through the surface of the glands (Studer-Thiersch, 1963). In penguins, the male incubates an egg for two months while the female is out at sea feeding, and if the female has not returned by the time the chick emerges, the male can feed it for a few days on milk secreted by the esophagus. Unlike milk production in mammals, both sexes of birds produce crop milk, and in both sexes, the hyperplasia is complete, and “milk” begins to be produced days before the hatch. What exactly signals this in either the male or the female is unknown, but prolactin is certainly important in both sexes (Silver 1984). Global gene expression profiling showed that gene expression patterns were also distinctly different in the ‘lactating’ crop as compared to the non-‘lactating’ crop, including a pigeon ‘milk’ growth factor with biological activity similar to epidermal growth factor, transferrin, and lactoferrin (Gillespie et al., 2011).

Dr. Pesavento’s next presentation was tissue from a Gouldian finch. After viewing Figures 3E and 3F, the audience members were asked to choose the best diagnosis. The most favored result was “I don’t know” (25%). The next three audience votes were almost evenly split between normal feeding accoutrement (18%), normal mating accoutrement (17%) and fibropapillomas (16%). Diagnoses with fewer votes were normal eye ornamentation (10%), normal acoustic accoutrement (7%) and fibromas (7%). The correct diagnosis was normal feeding accoutrement. As for the first case, it seemed that not very many audience members had any prior experience with this tissue type.

Figure 3E is the head (with open maxilla and mandible) of a Gouldian finch nestling, demonstrating an oral commissure mouth ornamentation that is present in nestlings and that disappears prior to full plumage. Nodules of loose fibrous tissue are at the commissures of the beak. The covering epithelium is thinned at the surface, and the subepithelium has

closely arranged collagen fibers. The fibrous tissue is basically acellular except for occasional fibrocytes (Figure 3F). The collagen fibrils are organized into lamellae that branch and interconnect with adjacent lamellae alternately parallel and perpendicular with the surface. Over the central, grossly yellow nodule, the epithelial layer is completely unpigmented, whereas over the peripheral, grossly blue nodules, there are scattered, fairly regularly placed melanocytes (Figure 3G).

Gouldian Finches are beautifully colorful birds native to the Australian coast. They breed well in captivity but are, unfortunately, losing numbers in the wild. As adults, they have stunningly colorful plumage, but they do not start out that way. The color in a Gouldian finch baby is limited to nodular blue and yellow ornamentation at the commissures of their mouths (http://www.aqua.org/explore/animals/gouldian-finch, accessed 11/30/15). These reflective beads are reportedly a way for the finch parents to recognize where to target food since the nests are typically dark, deep holes in trees. They also have, like other finches, elaborate markings on their palate. There are different theories concerning the mouth markings in nestling finches. Each species has a unique pattern easily seen in a gaping chick. The high contrast marks are easily seen and might specifically identify the chicks in the nest from parasitic bird species. Some birds are able to distinguish and reject intruders by these markings.

Rick Prum, curator and scholar at the Peabody Museum at Yale, studies structural color in birds. He has published several articles that explain how color is produced by the arrangement of fibrous arrays of collagen and was extremely helpful in trying to negotiate this case (Prum and Torres, 2003; Prum and Torres, 2004; Prum et al. 1999). Dr. Prum suggested that this might be a structural color produced by arrays of parallel collagen fibers. Although they have published a few papers on this, there has never been a publication on the structural colors of baby bird mouths. However, this could be confirmed with transmission electron micrographs (TEMs) of the collagen inside these balls. His interest is in the distribution of melanosomes, which are usually seen underneath the collagen. However, in this case, the melanosomes appear to be mixed within the collagen. He also noted that, of further interest, is the yellow color, which is a carotenoid color of some kind. In skin, the carotenoid colors are sometimes “tuned” in with a structured collagen back scattering (LaFountain et al. 2015). Dr. Christopher Reilly (pathologist, UC Davis) and Dr. Ivan Schwab (ophthalmologist, UC Davis) equated these structures with a fibrous type of tapetum. The tapetal structure consists of alternating layers of high and low refractive index material (collagen or cellular rodlets) whose thicknesses are compatible with wavelengths of light (Braekevelt 1999). At each interface in this structured arrangement a proportion of the incident light is reflected. So the thickness of the layers, the arrangement of the layers, and the presence (or absence) of melanocytes all contribute to the reflection/color.

Dr. Pesavento’s final case was tissue from a Bluefin tuna. After viewing Figure 3H, a gross image of the liver, the audience was asked to vote. The voting choices and results were “I don’t know” (24%), heat exchanger (17%), congestion (12%), capsular trauma/repair (10%) and salt gland (7%). The correct answer for this structure was heat exchanger.

Tunas and some other “warm-blooded” fishes and sharks (Lamidae) utilize countercurrent vascular retia mirabilia to conserve metabolic heat in order to maintain an elevated body temperature (Block and Stevens 2001; Fudge and Stevens 1996). This non-lesion was first brought to Dr. Pesavento’s attention by Dr. Corinne Davis (pathologist, UC Davis) as a normal visceral rete. A heat exchanger is a network of interdigitating arteries and veins (compare, for example, to the panpiniform plexus). The retia on the caudal surface of the liver are formed by massive branching of the celiac artery into parallel arteries that interdigitate with veins (Figure 3I). Vessels that leave the retia distally supply the stomach, cecum, intestine, and spleen and provide a thermal barrier between blood on the cardiac side of the exchange (cold) and venous blood (hot by food hydrolysis/metabolism) (Carey 1984; Cech et al., 1984). In the retia, countercurrent flow and the high surface area contact between the two blood supplies facilitate the transfer of nearly all of the metabolic heat in the venous blood to arterial blood. The retia prevents convective heat loss from the digestive system and enables temperatures in the viscera which can be as much as 15 degrees higher than the surrounding water. There are similar types of retia that warm the eyes of sharks and brains of ocean fish.

AN EXIGENT PANCREATIC TUMOR?

Dr. Ramesh Kovi (Experimental Pathology Laboratories Inc., Durham, NC) presented a unique lesion of pancreatic metastases of alveolar/bronchiolar (A/B) carcinoma in male F344 rats from a two-year carcinogenicity assay of tobacco specific carcinogens [NNK: 4-(methylnitrosamino)-1-(3-pyridyl)-1-butanone and NNAL: 4-(methylnitrosamino)-1-(3-pyridyl)-1-butanol] in drinking water that was conducted at the University of Minnesota Masonic Cancer Center (Balbo *et al.* 2014). The presentation also included an unpublished immunohistochemical characterization of neoplastic lesions in the lung and pancreas.

After viewing data on the group, dose, number of animals and duration of exposure (in weeks), as well as figures showing a metastatic carcinoma in the pancreas (data not shown), the audience was asked to choose the best diagnosis. 86% voted for a primary pancreatic tumor (i.e. ductular or acinar adenoma or carcinoma). Only 9% chose metastatic carcinoma and 5% chose “none of the above”. The majority of the audience voted for the diagnosis of pancreatic ductular carcinoma (41%), which was plausible based only on histomorphology. However, this was a metastatic lung tumor from rats treated with a potent tobacco-specific carcinogen. This lung alveolar/bronchiolar metastatic tumor resembled a pancreatic ductal tumor and, without specific knowledge of the chemical and concurrent lung tumor, would be easy to misdiagnose. However, the diagnosis of metastatic carcinoma was the correct diagnosis and was illustrated with further immunohistochemical characterization during the discussion using alveolar type II cell (prosurfactant protein C) and club (Clara) cell (CC10) specific markers.

Tobacco-specific carcinogens, including nitrosamines, play an important role in cancer induction by smoking or non-smoking tobacco products (Balbo *et al.* 2013; Hecht 1998). Tobacco-specific nitrosamines, such as 4-(methylnitrosamino)-1-(3-pyridyl)-1-butanone (NNK) and its metabolite, 4-(methylnitrosamino)-1-(3-pyridyl)-1-butanol (NNAL), are potent pulmonary carcinogens reported to play a role in the induction of exocrine pancreatic

tumors (Balbo *et al.* 2014; Rivenson *et al.* 1988). NNAL exists as enantiomers (*R*)-NNAL and (*S*)-NNAL due to the presence of chiral carbon atoms, and the carcinogenicity of these nitrosamines has been recently studied (Balbo *et al.* 2014).

In this study, male F344 rats were dosed in drinking water for 80 or 90 weeks with different tobacco-specific carcinogens (5 ppm NNK, 24 rats; 10 ppm racemic-NNAL, 15 rats; 5 ppm (*S*)-NNAL, 22 rats; 5 ppm (*R*)-NNAL, 24 rats). During the discussion, Dr. Kovi showed gross images of lung tumors depicting the extent of involvement of pulmonary parenchyma (Figure 4A) and gross images of lung tumors with extrapulmonary masses invading the mediastinum and thoracic cavity (Figure 4B). Treatment-related proliferative lesions were encountered in the lungs and pancreas (Table 3) (Balbo *et al.* 2014). The spectrum of histopathological lesions in the lung included alveolar/bronchiolar hyperplasia, adenoma and adenocarcinoma (Figure 4C) and multifocal malignant metastatic tumors in the pancreas affecting about 4.2% to 27% of rats treated with different tobacco-specific carcinogens (Figure 4D and Table 3). Immunohistochemistry was performed on the tissue sections of all tumors in the pancreas and lungs. All lung tumors and pancreatic tumors showed strong immunoreactivity for alveolar type II cell marker prosurfactant protein-C (PSP-C) and Clara (club) cell marker CC10 (Figures 4E–H).

In the human literature, 3–12% of all patients with diffuse metastatic disease have been reported to have pancreatic involvement (Showalter *et al.* 2008) and the five most common cancers with isolated metastases to the pancreas include renal, lung, breast, colon, and melanoma (Adsay *et al.* 2004). However, isolated pancreatic metastasis is extremely rare and not reported in rodents. Tobacco-specific carcinogen (NNK) induced pancreatic tumors were previously diagnosed as exocrine pancreatic ductular carcinoma based on histomorphology (Rivenson *et al.* 1988). In this study, further immunohistochemical characterization of tumors in the pancreas revealed that these tumors were metastatic alveolar/bronchiolar carcinomas.

In conclusion, Dr. Kovi stated that, in cases where pancreatic tumors have ductular epithelial morphology concurrent with carcinomas in the lungs, further characterization of tumor type should be considered to determine if the pancreatic tumors are pulmonary metastatic tumors.

The author would like to thank Drs. Steve Hecht and Gerry O’Sullivan at the University of Minnesota for providing the material used for presentation, and also acknowledges the anatomic pathologists at Experimental Pathology Laboratories Inc., in Durham, NC, and Dr. Kyathanahalli Janardhan at ILS, Durham, NC, for providing additional helpful consultation on these lesions.

INTRACRANIAL CONUNDRUMS I

Dr. James Morrison (Charles River Laboratories, Inc., Durham, NC) presented two rare and unusual intracranial neoplasms. The first case was from a Wistar Han male rat that was sacrificed moribund on study day 113 of a chronic two-year carcinogenicity bioassay. The lesion was grossly described as a pituitary mass. Dr. Morrison presented a series of four increasingly higher magnification, H&E stained images (Figure 5A) from the mass and then

asked the audience to vote on the best diagnosis. The voting choices and initial results were oligodendroglioma (38%), schwannoma (10%), neurocytoma (14%), pituitary adenoma (5%), ganglioneuroma (15%), neuroblastoma (14%), and other/I don't know (5%). Before sharing his preferred diagnosis with the audience, Dr. Morrison showed an additional series of images from immunohistochemically (IHC) stained slides and then asked for a revote. The IHC markers used included glial fibrillary acidic protein (GFAP), oligodendrocyte transcription factor 2 (Olig-2), neuronal nuclear antigen (Neu N), S100 beta, and synaptophysin. The neoplastic cells were positive for Neu N (Figure 5B) and negative for GFAP, Olig-2 (Figure 5C), and S100 beta. Fibrillary material was interspersed with the neoplastic cells that stained positive for synaptophysin (Figure 5D). After reviewing the IHC images, the audience revoted and the voting choices and results were oligodendroglioma (10%), schwannoma (4%), neurocytoma (37%), pituitary adenoma (7%), ganglioneuroma (5%), neuroblastoma (30%), and other/I don't know (7%). Dr. Morrison agreed with the majority of the participants that this neoplasm was a neurocytoma.

This represents the first reported case of a neurocytoma in the rat. Neurocytomas occur most commonly in humans, where they are typically low-grade neoplasms that most commonly afflict people under the age of 40 yrs. In humans, they are subcategorized as either central or peripheral, depending on whether they occur inside or outside of the central nervous system, respectively. Central neurocytomas are most common and typically occur intra-ventricularly, that is, they bulge into the lateral ventricles from the peri-ventricular parenchyma (Figarella-Branger et al., 2000). The lesion in this rat, although described as a pituitary mass, actually arose within one of the cranial nerves, as evidenced by the presence of a thin ring of myelinated axons surrounding the mass. As such it could be considered a peripheral neurocytoma if we were to attempt to categorize it using the human classification. Two case reports of central neurocytomas have recently been published in dogs (Huisinga M, et al. 2008; Rossmeisl JH, et al., 2012), but they have not been reported in other species to the author's knowledge.

Histologically, this neoplasm was composed of cells with small, round nuclei containing stippled chromatin and indistinct nucleoli. The neoplastic cells were arranged in small bundles and rows interspersed with eosinophilic, fibrillary material (Figure 5A). This material resembled neuropil, and although electron microscopy was not performed, it presumably represents the elaboration of cellular processes from the neoplastic cells, consistent with its positivity for synaptophysin (Figure 5D). Given the small, round nuclear morphology, the top differential diagnosis is an oligodendroglioma. However, while the nuclear morphology is similar between the two neoplasms, other features are present that allow for the two neoplasms to potentially be distinguished even without using immunohistochemistry. For example, the cell bodies of oligodendrogliomas that have been formalin fixed and paraffin embedded (which includes the majority of cases) typically have significant cytoplasmic clearing, imparting what is commonly referred to as a 'fried egg' appearance to the cell bodies. This is not an in situ change, but is instead a useful artifact. In addition, rat oligodendrogliomas also tend to have considerable endothelial hypertrophy and hyperplasia, with the vessels becoming very prominent and tortuous (commonly referred to as vascular garlands or glomeruloid vessels). In addition, a subset of oligodendrogliomas contain considerable eosinophilic to pale basophilic material separating clusters of

neoplastic cells. The material superficially resembles the fibrillary material in the neurocytoma but with important differences. In the oligodendroglioma, it is fairly amorphous, lacking the fibrillary appearance that is present in the neurocytoma. The material represents ground substance that is elaborated by the neoplastic cells (Weber, et al., 2011). It often contains mucin, which imparts a pale basophilic hue to the material in the histologic section. This is in contrast to the fibrillary material in the neurocytoma, which is uniformly pale eosinophilic and fibrillary (Figure 5A). If the above features are not prominent, immunohistochemistry can be used for a definitive diagnosis. Since neurocytomas are a neoplasm of the neuronal lineage, they stain positively for neuronal nuclear antigen (NeuN) and synaptophysin and negative for glial and schwann cell markers, including GFAP, Olig-2, and S100 beta.

The second case was presented on behalf of Dr. Katsuhiko Yoshizawa and Dr. Takayasu Moroki of Maruho Co., Ltd. of Kansai Medical University in Osaka, Japan. It was from a control male Sprague-Dawley rat that was sacrificed moribund at 55 weeks on study. It was grossly described as a pituitary mass firmly attached to the sphenoid bone (Figure 5E). Dr. Morrison presented a series of increasingly higher magnification images of the neoplastic cells (Figure 5F) and then asked the audience to vote for the best diagnosis. The voting choices and results were malignant astrocytoma (8%), malignant schwannoma (17%), histiocytic sarcoma (21%), pituitary carcinoma (10%), malignant pituicytoma (30%), rhabdomyosarcoma (12%), and other/I don’t know (2%). Before revealing the preferred diagnosis to the audience, Dr. Morrison showed additional immunohistochemically stained slides for vimentin (Figure 5G) and GFAP (Figure 5H), both of which showed strongly positive staining, and then asked the audience to revote. The voting choices and results were malignant astrocytoma (51%), malignant schwannoma (15%), histiocytic sarcoma (4%), pituitary carcinoma (1%), malignant pituicytoma (21%), rhabdomyosarcoma (1%), and other/I don’t know (4%). Although the audience shifted their diagnosis to a malignant astrocytoma after viewing the positive GFAP staining, their initial diagnosis of a malignant pituicytoma was correct, since pituicytomas are the only neoplasm consistently positive for GFAP in the rat.

Dr. Yoshizawa and his colleagues performed immunohistochemical staining on this case against a panel of markers which included vimentin (for mesenchymal cells); cytokeratin (for epithelial cells); GFAP (for astrocytes and pituicytes); S100 (for Schwann cells); ED1 (for microglia/macrophages); PCNA (proliferation marker); alpha smooth muscle actin, desmin, myoglobin (for muscle); prolactin, thyroid stimulating hormone (for pituitary epithelial cells); and melan A (for melanocytes). The neoplastic cells were strongly positive for vimentin, GFAP, and PCNA, weakly positive for S100 and ED1, but were negative for the remaining markers. This staining pattern is consistent with a neoplasm arising from the pituicytes of the pars nervosa of the pituitary.

Pituicytes are modified astrocytes of the pars nervosa that help to regulate the storage and secretion of anti-diuretic hormone and oxytocin (Hatton, 1988). By definition neoplasms of these specialized cells are called pituicytomas and they have been reported rarely in mice, rats, cats, dogs, and primates, including humans (Tekeli, et al., 1997; Satoh, et al., 2000; Moroki, et al, 2015; Zaki, et al., 1975; HogenEsch, et al., 1992; Figarella-Branger, et al.,

2002). In the rat, they are typically low-grade neoplasms, although local invasion is often present. This is the first known case of a malignant variant in the rat.

Differential diagnoses of benign pituicytomas include other spindloid neoplasms of the ventral brain, including fibrous meningioma, glioma and schwannoma. Differential diagnoses also considered for this malignant pituicytoma include pituitary carcinoma, histiocytic sarcoma, and rhabdomyosarcoma, all of which were excluded by the panel of IHC markers.

MAMMARY GLAND DEVELOPMENT: THE “WHOLE” STORY

Dr. Erin Quist (NIEHS, NTP, Research Triangle Park, NC) presented basic diagnostic criteria for assessing changes observed in the developing mammary gland and emphasized the importance of the mammary gland whole mount as a diagnostic tool in juvenile toxicity studies. After a brief introduction, the audience was asked to vote on two different cases from 21-day-old Sprague Dawley (SD) rats exposed to either ethinyl estradiol (EE_2) or bisphenol A (BPA) from gestation day 6 to postnatal day 90 (Delclos et al. 2014). Photomicrographs of mammary gland whole mount preparations were displayed for voting without revealing the dosing agent for each case; a photomicrograph of a mammary gland whole mount from an age-matched control animal was also included with each case for comparison. While the majority of the audience correctly identified that the first case (the BPA-treated animal) exhibited delayed mammary gland development (65%), a fair number of the voting participants felt that the observed changes were within normal limits (31%); only 4% thought development was accelerated compared to the untreated control. For the second case (the EE_2-treated animal), an overwhelming 86% of the audience agreed that mammary gland development was accelerated compared to the untreated control.

In the United States, breast cancer is one of the most common cancers in women, second only to lung cancer in female cancer-related deaths. It is estimated that 1 in 7 women will be diagnosed with breast cancer within their lifetime with over 294,000 new breast cancer cases and 40,290 breast cancer-related deaths projected for 2015. Although male breast cancer is far less common, the incidence is about 0.14% among American men with an estimated 2,350 new cases of invasive male breast cancer and 400 breast cancer-related deaths reported for this year (Howlader et al. 2015, American Cancer Society 2015). A strong relationship between hereditary factors and development of breast cancer has been well established (American Cancer Society 2015). However, most breast cancers occur in women with no family history of breast cancer, indicating that the environment plays an important role in the development of this disease (IBCERCC 2013).

The mammary gland develops primarily after birth and exhibits structural similarities across species at various stages of development (Davis and Fenton 2013). Human and rodent mammary glands develop at a similar biological pace for each developmental stage including infancy, childhood, puberty, adulthood and late life, validating the usefulness of the rodent model for breast cancer research. Also similar to humans, rodent terminal end buds (TEBs) are important in pubertal development, comprised of stem cells that proliferate and differentiate into terminal ductal lobular units (TDLUs). TDLUs are hormone-sensitive

precursors of the functioning mammary gland and the site of origin for most mammary cancers in women (IBCERCC 2013).

Developmental scoring of the mammary gland is best achieved via mammary gland whole mount preparation as it allows for visualization of the entire gland (Davis and Fenton 2013). Typically, the 4^{th} and 5^{th} glands are collected at the time of necropsy for whole mount evaluation, using the inguinal lymph node as an anatomical landmark. Collected glands are then laid flat on a glass slide, fixed in Carnoy's solution, cleared in xylene and stained with carmine alum stain in a process that takes up to 48 hours depending on the thickness of the gland. Cover-slipped whole mount preparations can be adequately evaluated under a dissecting microscope at 10× magnification (Davis and Fenton 2013, Plante et al. 2011). The developmental score is determined by characterizing the following features: (1) lateral growth (width of the gland) (2) longitudinal growth (as the gland matures the ducts and branches will extend upward toward and, in some cases beyond, the inguinal lymph node), (3) the number of primary ducts arising from the nipple, (4) budding (branch density), (5) lateral (side) branching, (6) the number of TEBs, and (7) the distance between the 4^{th} and 5^{th} glands (as the gland matures the 4^{th} and 5^{th} glands will grow together filling the space between them) (Figures 6A and 6B) (Davis and Fenton 2013). The developmental scoring scale typically ranges from 1 to 6, where age-matched control tissues (Figure 6A) will typically be graded as 3 and glands exhibiting delayed (Figure 6C) or accelerated (Figure 6D) development will receive scores less than or greater than 3, respectively. In the examples presented here, the mammary gland depicted in Figure 6C received a score of 1 due to marked decreases in all the scoring parameters described above, relative to the control tissue in Figure 6A. The mammary gland in Figure 6D is clearly very dense with increased lateral and longitudinal growth, as well as increased budding and number of TEBs compared to the untreated control and was thus graded as 6.5.

When viewed side by side, it is easy to appreciate the advantages and disadvantages of evaluating the mammary gland via whole mount (Figure 6E) or histological examination (Figure 6F). While the whole mount preparation allows visualization of the entire gland for structural assessment, cellular features of the mammary gland are best evaluated via histological examination of coronal mammary gland sections (Davis and Fenton 2013). In the female rat and mouse, the glandular structures of the mammary tissue are typically tubuloalveolar in their morphology (Figure 6F) and the male rat gland is described as being lobuloalveolar, which is also the predominant glandular morphology in pregnant and lactating females (Figure 6G). However, prenatal exposures to estrogenic compounds may induce a conformational change in the male glandular morphology in which "feminization" of the gland occurs leading to the more female tubuloalveolar morphology (Figure 6G inset). Histological evaluation of mammary gland whole mount preparations is also recommended when abnormally thickened ducts and/or branches are observed (Figure 6H). These changes may indicate inflammation, ductular hyperplasia or neoplasia. However, histology is required to make a definitive diagnosis. Tissues already fixed and stained for whole mount preparation may also be paraffin-embedded and processed for histopathology (Plante et al. 2011).

The mammary gland whole mount is a simple and useful diagnostic tool that can provide valuable information regarding structural changes in the developing mammary gland, and is especially important for the assessment of developmental abnormalities in juvenile toxicity studies and studies involving endocrine disruption. While histology is critical for evaluating the morphologic features of cellular populations within the gland, the entire structure of the mammary gland cannot be visualized using this technique. Therefore, it is recommended that mammary gland whole mounts be used in conjunction with histopathology for a complete evaluation. It is also important to sample both male and female mammary glands in the rat model, as changes in structure and cellular morphology may be present in both sexes; mammary glands in male mice regress at an early age and are therefore not a reliable indicator for developmental abnormalities.

The author would like to thank Drs. Suzanne Fenton, Schantel Hayes-Bouknight and Adam Filgo for select images and Ms. Beth Mahler for photographic support.

CANINE AND RODENT PULMONARY PATHOLOGY: ARE THEY THE SAME OR DIFFERENT? AN ULTRASTRUCTURAL CASE STUDY

Dr. Kathleen Szabo (Charles River Laboratories, Inc., Durham, NC) presented ultrastructural cases in dogs and rats as a diagnostic challenge. Three sets of transmission electron microscopy (TEM) cases were presented for voting followed by an overview of normal alveolus ultrastructure and a discussion of phospholipidosis. The TEM images of formalin fixed lung tissue were from two separate one-month oral gavage studies conducted with an undisclosed test article in male and female Beagle dogs and Han Wistar CRL:WI(Han) rats.

The challenge of the first set of images in treated animals was to identify the cell(s) present in the electron micrographs based on ultrastructural appearance at magnifications of 15,500× in the dog (data not shown), and 10,700× in the rat (Figure 7A). The potential diagnostic choices and voting results for the dog and rat were alveolar macrophage (53%), type II pneumocyte (39%), type I pneumocyte (7%), neutrophil and fibroblast (1% each), lymphocyte and other (0% each). The majority of the audience chose the correct answer, alveolar macrophage, based on ultrastructural appearance and location within the alveolar space.

In the second set of images, the challenge in treated animals was to formulate a diagnosis for the changes observed ultrastructurally in the cytoplasm of the alveolar macrophage at magnifications of 10,700× in the dog (Figure 7B), and 35,900× in the rat (**data not shown**). The potential diagnostic choices and voting results for this set in the dog and rat were phospholipidosis (37%), increased lamellar bodies, lysosome (29%), accumulation of membrane remnant material, lysosome (13%), increased whorled material, lysosome (11%), myelin figures (9%) and finally other (0%). Dr. Szabo stated that her preferred diagnosis was “alveolar macrophage: accumulation, membrane remnant material, lysosome” as this was a descriptive instead of an interpretative diagnosis. She did understand the majority vote for an interpretive diagnosis of phospholipidosis. Dr. Szabo recommended using a descriptive diagnosis for the electron micrographs and, after having taken into consideration the

additional pathological features needed for definitive diagnosis, reserving interpretation for the narrative of the report.

The final image was from a treated dog at 10,700× magnification (**data not shown**), and similar to Case 2 the challenge was to formulate a diagnosis, but this time the audience was not provided a specific cell type. The majority (55%) voted for alveolar macrophage: accumulation, membrane remnant material, lysosome with aggregation. Alveolar type II pneumocyte hyperplasia and alveolar histiocytosis tied in second place with an audience vote of 16% each, followed by 13% for alveolar macrophage aggregation and 1% for other. Dr. Szabo stated that while she did understand the majority vote of the audience, her preferred diagnosis was alveolar macrophage aggregation based on the overall perspective gained from evaluation of the entire set of electron micrographs in the study and review of the toluidine blue stained thick sections; the audience did not have this same perspective. Importantly, the terminology “alveolar macrophage aggregation” is consistent with INHAND (International Harmonization of Nomenclature and Diagnostic Criteria for Lesions in Rats and Mice) nomenclature for this type of finding in the lung (Renne et al. 2009, p. 31S).

Then, Dr. Szabo proceeded to comment on the study data. The finding of lysosomal accumulation of membrane remnant material was similarly present in both the dog and rat studies when examined ultrastructurally, and a minor difference was that macrophage aggregation was observed ultrastructurally in the dog lung.

Next, an overview of normal pulmonary ultrastructure focusing on the alveolar wall began with an electron micrograph at 15,500× magnification of a control female dog lung. Individual cell types of the alveolar wall were then shown ultrastructurally and discussed. The type I pneumocyte is simple squamous epithelium that is part of the alveolar wall and recognizably thin on ultrastructure. There is a fused basal lamina between the type I pneumocyte and the endothelial cell that along with surfactant forms the blood-air barrier (Cross and Mercer 2002). The type II pneumocyte, located at the “branching point of the alveolar septum” (Young and Heath 2000, p. 232), is cuboidal epithelium that contains lamellar bodies, has surface microvilli, and plays a reparative role in alveolar wall damage through division and/or differentiation into type I pneumocytes (Cross and Mercer 2002; Young and Heath 2000). The alveolar macrophage is typically seen in the alveolar space or near the alveolar wall on ultrastructure. An important distinguishing feature is cytoplasmic pseudopodia; the cytoplasm contains typical organelles, including lysosomes in various stages, and mitochondria (Cross and Mercer 2002).

The next part of the presentation centered on some examples in which lamellar bodies are seen or induced. Lamellar bodies are normally observed in the lung type II pneumocyte, stomach mucosal epithelium, and tongue papillae, among other cell types (Schmitz and Müller 1991). Also, lamellar bodies can be observed in lysosomal storage diseases (e.g. Niemann-Pick, Tay-Sachs) (Halliwell 1997) and are induced in the alveolar macrophages of rats that have undergone hypophysectomy (Renne et al. 2009). The literature reports greater than 50 cationic amphophilic drugs can cause drug-induced phospholipidosis (Cartwright et al. 2009; Halliwell 1997). These drugs span numerous therapeutic classes (e.g.

antidepressant/SSRI, antibiotic, antimalarial, etc.) but share common physiochemical properties (Halliwell 1997; Reasor et al. 2006).

The remainder of the presentation centered on phospholipidosis, which Halliwell (1997, p. 53) stated is “an excessive accumulation of intracellular phospholipids”. On histopathology, phospholipidosis can be suspected in cases of foamy cytoplasmic vacuolation in a wide variety of cells, with single or multiple tissue involvement (Halliwell 1997; Cartwright et al. 2009; Chang et al. 2014). Phospholipidosis may be subcategorized into “macrophage-dominant”, “parenchymal cell-dominant”, and “localized” (Ettlin et al. 2010, p. 221). The macrophage type consists of accumulation of foamy macrophages in lung, hematopoietic tissues, and liver. Cells of parenchymal organs (e.g. hepatocytes) accumulate phospholipid in the parenchymal cell dominant type. Localized phospholipidosis is a subcategory of the parenchymal type, and Ettlin et al. (2010, p. 221) states that it “probably reflects exposure of the affected organ to a higher concentration of the drug”.

In general, the diagnosis of phospholipidosis cannot be established by using electron microscopy as a stand-alone technique. Histopathology results in various organs, examination of toluidine blue-stained thick sections and immunohistochemistry may provide elements to confirm suspicion. Comparison of control to treated samples may reveal an excessive amount of whorled material present within secondary lysosomes in cases of suspect phospholipidosis. Ultrastructurally, affected lysosomes may vary in size and may appear enlarged due to the accumulation of whorled material (Cartwright et al. 2009). The lamellae can be unicentric, multicentric, tightly wound, or associated with a variable matrix (Reasor et al. 2006). Differences may exist that influence phospholipid accumulation to include species, strain, and age of laboratory animals, specific tissue affinity, metabolic rate of the drug and its metabolites, dose and duration of the test article, other drugs taken concurrently, and the drug itself (Halliwell 1997; Ettlin et al. 2010).

Ultrastructural variability can be present in lamellar bodies and differences may exist between species and organs affected and in size and composition of lamellae (Anderson and Borlak 2006). Knowledge of normal pulmonary ultrastructure is important when evaluating electron microscopy images of the lung as well as comparison to control animals.

In conclusion, electron microscopic micrographs of lung from treated rat and dog representing a diagnostic challenge were presented. A descriptive diagnosis of “alveolar macrophage: accumulation, membrane remnant material, lysosome” was proposed. Normal ultrastructure of the lung was reviewed and variations in ultrastructural appearance of lamellar bodies and ultrastructural morphological features of phospholipidosis were discussed based on the literature. In most cases, descriptive diagnoses are preferable over interpretative diagnoses for electron micrographs.

IMPRINTS, SMEARS AND PREPS – OH MY!

Dr. Jennifer Neel (College of Veterinary Medicine, North Carolina State University, Raleigh, NC) presented two challenging cytology cases to an audience that consisted primarily of veterinary anatomic pathologists. The first case was from an 8-year-old neutered, male

domestic shorthair cat that presented to the North Carolina State University Veterinary Hospital for evaluation of a four-month history of weight loss, decreased appetite and lethargy. The cat was kept indoors only since adoption at a young age and was FeLV/FIV-negative. On physical exam, he was thin with diffuse muscle atrophy, temperature/pulse/respiration were within normal limits, peripheral lymph nodes were prominent, and anisocoria with no left menace response was noted. Routine bloodwork showed a moderate, normocytic, normochromic, non-regenerative anemia (HCT 21.2, reference interval 32.8–49.8%, reticulocyte count 12, 339 cells/μl) but was otherwise unremarkable. A complete ophthalmology exam showed complete (right) to multifocal (left) retinal detachment with petechial hemorrhage. An abdominal ultrasound exam revealed diffuse hepatosplenomegaly with hepatic and sternal lymphadenopathy, most consistent with an infiltrative or multicentric disease such as lymphoma. Images of a liver aspirate were shown (Figures 8A–D), and the audience was polled for their interpretation with the following results: 11% phagocytized cellular debris / endogenous material; 12% phagocytized foreign material; 3% storage disease; 17% large granular lymphoma; 35% degenerating protozoa; 22% degenerating yeast. The correct answer was ‘degenerating yeast’ due to an infection with *Histoplasma capsulatum*.

Key features of the cytology aspirate were reviewed. From low power, the clusters of uniform hepatocytes were clearly visible together with many inflammatory cells. On higher power, it could be seen that the inflammatory cells consisted primarily of histiocytes and slightly degenerate neutrophils, with lesser numbers of small mature lymphocytes, plasma cells and occasional large lymphocytes. In the background and within histocytes, low but consistent numbers of round, 2 to 5μm diameter organisms with a thin clear cell wall, light blue interior and a dark blue, eccentric nucleus (½ full, ½ empty appearance) were observed (Figures 8C & E). Within many histiocytes, and free in the background, round, approximately 5μm diameter structures with a stippled to frothy, purple/pink interior were noted and interpreted as degenerating or partially degenerating fungal organisms (Figures 8D, F & G). Distorted, fragmented and poorly stained ‘ghost’ forms of *Histoplasma* have been reported in residual nodules (histoplasmosis) in humans (Chandler et al., 1987).

Structures similar in appearance to the presumed degenerating fungal organisms were discussed (Figures 8H–J) and included: (1) a ruptured neoplastic granular lymphocyte with swollen granules was shown, (2) a peripheral blood neutrophil with phagocytized mast cell granules from a dog with mast cell disease was also shown; the ingested granules appeared swollen and ring-like (Figure 8H), (3) ragocytes from a dog with autoimmune disease (ragocytes are phagocytic cells with ingested immunoglobulin, fibrin and complement) (Figure 8I) and (4) peripheral blood neutrophils with presumed ingestion of lubricant material were shown and, again, had a somewhat similar appearance (Figure 8J). This last example was a blood smear was from a cat with a urethral blockage. Based on the timing of the attempt to pass a urinary catheter, the appearance of the material in peripheral blood and the subsequent resolution of the finding on later blood smears, it was thought that embolization of lubricant occurred during the procedure.

Potential differentials for *Histoplasma sp.* were discussed (Chandler et al., 1987). *Candida* yeast can overlap in size, however, they typically have a solid blue interior, are more likely

to be oval forms, and often form pseudohyphae. *Candida glabrata*, in particular, can look similar to *Histoplasma capsulatum* because the yeast forms are often the only forms appreciated, but they also tend to have a very solid interior compared with the '½ full, ½ empty' appearance of *Histoplasma sp*. Poorly or non-encapsulated *Cryptococcus* spp. could also appear somewhat similar to *Histoplasma sp.*, however it tends to be more variably-sized and also lacks the differential internal staining seen with *Histoplasma*.

Can histiocytes kill *Histoplasma* organisms? Evidence shows that when macrophages initially ingest the organisms, they are ineffective at killing (Newman 1999). However, studies with human dendritic cells show that they are capable of phagocytizing, killing and degrading the yeast (Gildea et al., 2001) (Thind et al., 2015). This results in triggering of cell-mediated immunity, which, in turn, causes activation of macrophages allowing for effective killing (Porta et al., 2000).

This cat was treated with itraconazole and initially did well, but eventually presented for recurrence of similar signs. A clinical workup showed no evidence of histoplasmosis on cytology aspirates of multiple organs. The owners then elected to do an itraconazole trial and the case was lost to follow-up.

Important take-home points were discussed. The CBC is actually a very insensitive indicator of inflammation; in this patient with significant inflammation of the liver, the WBC findings were unremarkable. While the appearance of the presumed degenerating organisms in the context of mixed inflammation should inspire a thorough search for an agent, other materials such as degenerating granules or phagocytized endogenous or exogenous material could look similar.

The second case presented by Dr. Neel was from a 3-year-old, male, castrated Labrador retriever dog. He presented to the North Carolina State University Veterinary Hospital for evaluation of a 1–2 month history of decreased appetite and lethargy. On physical exam, he was mildly febrile (103 F) with a pulse of 120 bpm and was panting. His mandibular, prescapular and popliteal lymph nodes were mildly enlarged. Initial diagnostics included lymph node aspirates and a CBC. The audience was shown images of the lymph node aspirates (Figures 8K–M) and then polled with the following results: 1% lymphoid hyperplasia; 6% lymphoid hyperplasia with inflammation; 23% lymphoid hyperplasia with extramedullary hematopoiesis (EMH); 10% lymphoma; 12% lymphoma with inflammation; 23% lymphoma with EMH; 23% myeloid leukemia; 1% other / I don't know. A limited amount of data from the CBC was then revealed including a total WBC count of 95.13 × 10^3/μl (RI 4.39–11.61 × 10^3/μl]) and a hematocrit of 31.2% (RI 39.2–55.9%). In addition, the audience was shown a representative image of the peripheral blood smear (Figure 8N) and was then re-polled and with the three most popular choices then being 61% for myeloid leukemia, 11% for lymphoma with EMH and 9% for lymphoma with inflammation. Myeloid leukemia was the correct response. In addition to the blood work and cytology images, flow cytometric analysis findings of peripheral blood were discussed. Results of this test showed that 86% of the gated abnormal population was positive for CD14, 10% was positive for CD4 and all cells were CD34 negative. These findings, together with the

cytology and CBC findings, were interpreted as consistent with chronic monocytic or myelomonocytic leukemia.

Cellular features in the lymph node aspirate that suggest myeloid differentiation include nuclei that are variably shaped including band, bean, indented, and lobulated, together with a chromatin pattern that is quite fine and dispersed. The relatively high numbers of larger, less mature forms with nuclei that are atypical for normal immature myeloid cells (lobulated or pleomorphic) lead away from benign EMH and towards a diagnosis of leukemia. The peripheral blood picture is one of leukemia with very high numbers of abnormal leukocytes. Evidence of monocytic differentiation is seen; cells contain nuclei that are pleomorphic to lobulated and often have a few small vacuoles. There is, essentially, a lack of very immature cells containing visible nucleoli, indicating that this is a more chronic form of leukemia versus an acute myeloid leukemia.

In human medicine, extramedullary myeloid proliferations can occur with acute myeloid leukemia (AML), myelodysplastic syndrome (MDS) or myeloproliferative neoplasms (MPN). These proliferations may or may not form a mass in tissues. When they do, the mass can be termed a myeloid sarcoma, which typically consists of myeloblasts with or without maturation and, by definition, forms at a site other than bone marrow. In this case, histopathology was not performed so we were unable to confirm if a mass lesion was present or if the neoplastic cells followed an infiltrative pattern. In humans, common sites of extramedullary myeloid proliferations include skin, lymph node, the vertebrae and the GI tract. Extramedullary myeloid proliferations can occur in aleukemic and subleukemic leukemias and are considered an indication for bone marrow screening in those patients without peripheral blood evidence of neoplasia (Campidelli et al., 2009). Although uncommon, extramedullary myeloid proliferations have been reported without evidence of current or previous leukemia. While extramedullary myeloid proliferations are nearly always composed of neoplastic cells, cases of proliferations composed of benign cells have been reported. Pyoderma gangrenosum, thought to represent an immune system dysfunction of neutrophils resulting in cutaneous ulcers and, potentially, infiltration of other organs, can be associated with AML, as well as many other conditions, and is considered by some to be an indication for bone marrow screening (Braswell et al., 2015).

In this case, the owner declined chemotherapy and the patient was lost to follow up. Important take home points were that leukemic cells in AML, MDS and MPN can infiltrate tissues (extramedullary myeloid proliferations) and may be termed a myeloid sarcoma if the infiltrates form a mass. These proliferations can be a challenge to distinguish from benign EMH, inflammation or lymphoma / other neoplasms. When identified or suspected, extramedullary myeloid proliferations should inspire evaluation of the peripheral blood and/or bone marrow.

NEUROPATHOLOGY TEXAS-STYLE

Dr. Brian Porter (Department of Veterinary Pathobiology, Texas A&M University, College Station, TX) presented three diagnostic neuropathology cases. The first case involved a 2-year-old, neutered male Mastiff that presented with a history of fever and progressive

tetraparesis. Neurologic examination revealed intermittent extensor rigidity in all four limbs and hyperreflexia in the rear limbs. Following anesthesia for a myelogram, the dog developed grand mal seizures and died.

The audience was shown low and high magnification images (Figures 9A and 9B) of the spinal cord and then asked to vote on the etiology. The voting choices and results were *Leishmania infantum* (24%), *Histoplasma capsulatum* (17%), *Neospora caninum* (17%), *Trypanosoma cruzi* (14%), *Toxoplasma gondii* (14%), *Sarcocystis neurona* (11%), and finally *Encephalitozoon cuniculi* and *Hepatozoon americanum* (each at 1%). The correct answer was *Trypanosoma cruzi*. The lack of a clear majority vote for this and the other cases presented by Dr. Porter may have been due to the mix of both clinical and anatomic pathologists and toxicologic pathologists in the audience as well as a mix of both novice and seasoned pathologists.

Dr. Porter then discussed the specifics of this case. At necropsy, the right cerebral hemisphere was slightly swollen with flattened sulci. Discolored foci were evident in the white matter of the cervical spinal cord. Histologically, random multifocal areas of granulomatous inflammation were scattered throughout the central nervous system, most severely in the brain stem and spinal cord (Figure 9A). Inflammatory foci were composed of macrophages, fewer lymphocytes and plasma cells, and rare neutrophils. Within the cytoplasm of occasional macrophages were multiple protozoal amastigotes with a kinetoplast (Figure 9B). Similar inflammation and organisms were evident in the spleen and heart, although cardiac involvement was very mild. The morphology of the organisms at the ultrastructural level was compatible with *Trypanosoma cruzi* (data not shown).

American trypanosomiasis, or Chagas' disease, is caused by the protozoal hemoflagellate *Trypanosoma cruzi* (Bern 2015; Esch and Peterson 2013). The parasite is transmitted to humans when the feces of the triatomine vector is inoculated during a blood meal or contacts a mucous membrane. Trypomastigotes in the bloodstream enter nucleated cells, especially myocardiocytes, and develop into amastigotes. After the organism replicates, infected cells rupture and release amastigotes, which return to the trypomastigote form and reenter the bloodstream. Chagas' disease is endemic throughout Central and South America, and the most important consequence of infection is cardiomyopathy, which occurs in 20–30% of infected people. It is estimated that approximately 300,000 people are infected in the United States, and although most of those infections were acquired in other countries, locally acquired infections have been reported.

In dogs, *T. cruzi* infection causes a fulminating myocarditis with death from acute heart failure (Williams et al. 1977). Gross lesions include dilation of the right ventricle and atrium and pale foci within the myocardium. Histologically, affected dogs have lymphoplasmacytic and histiocytic myocarditis with necrosis and intramyocardiocyte pseudocysts containing amastigotes. Involvement of other organs is infrequently seen. This case was unusual in that lesions were much more severe in the central nervous system than they were in the heart. The major differential diagnosis with organisms having this morphology is *Leishmania*, which closely resembles *T. cruzi*.

The second case involved an adult cow with a history of unspecified neurologic signs. After viewing a series of images (Figures 9C and 9D as examples) of the cerebellum, the audience was asked to vote on the etiology. The voting choices and results were *Solanum* toxicity (19%), delayed organophosphate toxicity (16%), *Phalaris* toxicity (15%), selenium toxicity (13%), mercury toxicity (13%), mesquite toxicity (12%), cycad toxicity (9%) and bromethalin toxicity (3%). Although there was not clear majority vote, the etiology garnering the most votes, *Solanum* toxicity, was the correct answer.

The cow in this example developed neurologic signs following ingestion of *Solanum dimidiatum* (western horsenettle). Gross lesions were not evident at necropsy, and histologic lesions were limited to the cerebellum. Cerebellar folia in some areas were thinner than normal (Figure 9C). Purkinje cell neurons were swollen and finely vacuolated with eccentric nuclei (Figure 9D). Many Purkinje cells were lost and replaced by proliferating Bergmann's glia. Purkinje cell axons within the granular cell layer were occasionally swollen (torpedoes). With Holmes silver stain, missing Purkinje cells were occasionally highlighted by staining of basket cell axons, so-called "empty baskets."

The plant genus *Solanum* is large and diverse, containing common garden plants such as tomatoes and potatoes. Some members of the genus cause cerebellar degeneration in ruminants, including *Solanum dimidiatum* (Menzies et al. 1979), *Solanum bonariense* (Verdes et al. 2015), *Solanum kwebense* (van der Lugt et al. 2010), *Solanum subinerme* Jack (Lima et al. 2014), and *Solanum paniculatum* (Guaraná et al. 2011) in cattle, and *Solanum cinereum* (Bourke 1997) and *Solanum viarium* (Porter et al. 2003) in goats. Clinical signs with chronic ingestion include ataxia, paresis, a wide-based stance, tremors, and a hypermetric gait. In Texas, toxicity associated with *Solanum dimidiatum* is most common in the west central part of the state, where it is referred to as "crazy cow syndrome."

The toxic principle responsible for *Solanum* toxicity is unknown. Ultrastructural examination has shown that swollen Purkinje cells contain membranous bodies, leading to the hypothesis that toxicity is an induced lysosomal storage disease resembling gangliosidosis (van der Lugt et al. 2010). It has also been suggested that the active principle of *Solanum* spp. forms a complex with lipid material that cannot be readily metabolized (De Barros et al. 1987). A recent study suggests that neuronal cytoskeletal abnormalities in affected Purkinje cells lead to altered axonal transport (Verdes et al. 2015).

The third case involved an approximately 1-year-old mixed breed heifer that became acutely recumbent and unable to rise. Physical exam revealed fever, decreased facial sensation, decreased patellar reflexes, and decreased withdrawal reflexes in the rear limbs. The heifer died despite supportive therapy.

The audience was shown a series of images (Figures 9E–F) of the spinal cord and asked to diagnose the etiology. The voting choices and results were clostridial myelitis (28%), West Nile virus (16%), bovine astrovirus (15%), pseudorabies virus (12%), bovine herpesvirus (10%), rabies virus (8%), Cache Valley virus (7%) and ovine herpesvirus 2 (3%). The correct etiology was bovine astrovirus.

Necropsy findings for this case were unremarkable, but histologic evaluation of the central nervous system showed inflammation within the cerebellum, brain stem, and spinal cord. Lesions included perivascular cuffing by lymphocytes and plasma cells, gliosis, and severe neuronal necrosis with neuronophagia (Figures 9E–F). The spinal cord was most severely affected. Fluorescent antibody testing for rabies virus was negative. In situ hybridization for bovine astrovirus strongly labeled the cytoplasm of spinal neurons.

The family *Astroviridae* is divided into two genera: *Mamastrovirus* (in mammals) and *Avastrovirus* (in birds). Astroviruses are one of the leading causes of diarrhea in human neonates worldwide, but even though they have been described in a wide variety of animal species, their role in animal disease is less clear (Moser and Schultz-Cherry 2005). In 2013, a novel bovine astrovirus was identified as a cause of encephalomyelitis in a Californian steer, and retrospective analysis of 32 cases of idiopathic bovine encephalitis identified three additional cases (Li et al. 2013). More recently, a similar neurotropic bovine astrovirus was reported in Switzerland and was associated with the same pattern of lesions (Bouzalas et al. 2014). In addition to cattle, astrovirus-associated encephalitis has been reported in immunocompromised humans (Brown et al. 2015) and in mink (Blomström et al. 2010).

The contributor would like to thank Dr. Fawzi Mohamed (USDA), who initially worked on the *Trypanosoma cruzi* case, and Drs. Kristin Eden (Virginia Tech University) and Patricia Pesavento (University of California-Davis) for assistance with the bovine astrovirus case.

INTRACRANIAL CONUNDRUMS II

In his second presentation, Dr. James Morrison (Charles River Laboratories, Inc., Durham, NC) presented another intracranial neoplasm. This case was from a Fischer 344 male control rat that was sacrificed moribund on week 93 of a chronic two-year carcinogenicity bioassay. Dr. Morrison presented a series of five increasingly higher magnification, H&E-stained images (Figures 10A and 10B) from the neoplasm and then asked the audience to vote on the best diagnosis. The voting choices and initial results were malignant astrocytoma (18%), malignant microglial tumor (33%), malignant glioma (30%), malignant reticulosis (12%), histiocytoma sarcoma (5%), and other/I don’t know (1%). Before sharing his preferred diagnosis with the audience, Dr. Morrison showed an additional series of images from immunohistochemically (IHC) stained slides and then asked for a revote. The IHC markers used were glial fibrillary acidic protein (GFAP; for astrocytes), ionized calcium binding adaptor molecule 1 (Iba1; for microglia/macrophages), major histocompatibility complex class II (MHCII; Ox-6 clone); for antigen presenting cells) and the *Ricinus communis* agglutinin 1 (RCA-1; for microglia/macrophages). The neoplastic cells were negative for GFAP (Figure 10C), and positive for Iba-1 (Figure 10D), MHCII (Figure 10E) and RCA-1 lectin (Figure 10F). After reviewing the IHC images, the audience revoted and the voting choices and results were malignant astrocytoma (2%), malignant microglial tumor (65%), malignant glioma (7%), malignant reticulosis (8%), histiocytoma sarcoma (18%), and other/I don’t know (0%). Dr. Morrison agreed with the majority of the participants that, based on the IHC staining pattern, the histogenesis of this neoplasm was most likely microglial, and so the diagnostic term “malignant microglial tumor” was most appropriate,

although histiocytic sarcoma, if designated as primary to the CNS, was also a reasonable alternative.

This case is representative of what has been traditionally diagnosed as an astrocytoma in the rat. Recent data, however, have called the histogenesis of this neoplasm into question. The diagnosis of a rat astrocytoma has historically been based on the histologic features of the neoplasm apparent on an H&E stained slide because, when immunohistochemistry is applied, the neoplastic cells are uniformly negative for astrocytic markers including glial fibrillary acidic protein (GFAP), glutamine synthetase and S100β (Krinke, et al., 2000; Weber, et al., 2011; Kolenda-Roberts, et al., 2013). However, there have been several recent publications that report positive immunohistochemical staining results of 'astrocytomas' in Fischer 344, Sprague-Dawley, and Wistar Han rats using markers against microglia/macrophages, including Iba-1, ED-1 (CD68), MHCII (Ox-6), RM-4, and the RCA-1 lectin (Nagatani, et al., 2009; Kolenda-Roberts, et al., 2013; Nakamura, et al., 2013). A brief summary of the findings and conclusions of each of these publications follows.

In Nagatani et al. (2008), the authors evaluated sixty-four cases in Sprague-Dawley and F344 rats that were diagnosed as malignant astrocytoma or malignant reticulosis. The neoplastic cells of all the neoplasms showed various immunoreactivities for RM-4, ED-1, and/or vimentin, and none showed any reactivity for GFAP or S-100 protein. The marker RM-4 specifically detects macrophage and dendritic cell populations residing in various organs and tissues, including microglia in the central nervous system (CNS) (Iyonaga, et al., 1997). The marker ED-1 is specifically expressed on various macrophage populations (Damoiseaux, et al., 1994), including microglia, and reportedly detects the rat homologue of the lysosomal protein CD68 (http://www.abcam.com/cd68-antibody-ed1-ab31630.html). The authors concluded that, from the results of morphological and immunohistochemical examinations, there are no distinctive differences between spontaneous astrocytomas and malignant reticulosis in rats and they are probably derived from the same cell lineage, most likely microglia or macrophages.

In Kolenda-Roberts et al. (2013), the authors examined twenty-eight spontaneously occurring glial tumors that were previously diagnosed as astrocytomas, oligodendrogliomas, and gliomas and characterized them using immunohistochemistry against RCA-1, Iba-1, MHC Class II, Olig2, GFAP, S100 beta, glutamine synthetase, neurofilament, and PCNA. This diverse list of markers allowed the authors to explore the histogenesis of the most commonly diagnosed glial tumors in the rat, but with a particular emphasis on astrocytomas. RCA-1, the *Ricinus communis* agglutin 1, is a plant lectin that has long been recognized to stain microglial and macrophage populations (Suzuki, et al., 1988). Iba-1 is a cytoplasmic actin binding protein that specifically localizes to microglia in the CNS (Ito, et al., 1998), although it stains other macrophage populations in other tissues. MHC Class II is expressed on antigen presenting cells, including macrophages, although the intensity of the staining is variable depending upon the developmental stage and degree of cellular activation. Olig2 is an oligodendrocyte lineage specific transcription factor that has been demonstrated to stain both normal and neoplastic oligodendrocytes (Zhou, et al., 2000; Kolenda-Roberts, et al., 2013; Rodriguez and Giannini, 2010). GFAP is an intermediate filament protein that has long been utilized as an astrocytic marker (Summers, et al., 1995). S100 beta protein is

expressed by a subset of mature astrocytes, specifically those that surround blood vessels (Wang and Bordey, 2008. Although S100 beta is used primarily as an astrocytic marker, low levels of expression have been reported in subsets of oligodendroglial cells (Hachem, et al., 2005). Glutamine synthetase is another marker of astrocytes and it catalyzes the conversion of glutamate and ammonia to glutamine (Wand and Bordey, 2008). As with S100 beta, however, expression of glutamine sythetase has also been noted in oligodendroglial cells (Cammer, 1990). Neurofilament is an intermediate filament expressed in neurons and PCNA is a commonly used proliferation marker.

Kolenda-Roberts, et al. determined that, of the original 14 neoplasms diagnosed as astrocytomas, none stained for any of the three astrocytic markers used. Nine of the neoplasms stained positive for RCA-1, Iba-1 and occasionally MHC Class II, and negative for GFAP, S100 beta and glutamine synthetase. The remaining neoplasms originally diagnosed as astrocytomas stained positive for Olig2 and were reclassified as oligodendrogliomas. The authors also applied the same IHC markers to a series of acrylonitrile induced glial neoplasms originally diagnosed as astrocytomas and the staining pattern was identical to that seen in the spontaneous neoplasms. The authors proposed the term ‘malignant microglial tumor’ for the series of neoplasms.

Lastly, in Nakamura et al. (2013), the authors used the IHC markers Iba-1 and CD-68 to examine four spontaneous neoplasms that were originally diagnosed as astrocytomas from one Wistar Hannover rat and three Sprague-Dawley rats. All four neoplasms were strongly positive for Iba-1, sporadically positive for CD-68 and negative for GFAP, Olig2, Vimentin, CD8, and neurofilament, consistent with the findings of the other two manuscripts described above.

To summarize, in the three manuscripts described above, both spontaneous and treatment-induced rat neoplasms originally diagnosed as astrocytomas were evaluated. All of the neoplasms were positive immunohistochemically for macrophage/microglial markers and none of the neoplasms were positive immunohistochemically for astrocyte markers. This pattern is consistent with a macrophage or microglial histogenesis of these neoplasms and is in sharp contrast to current diagnostic practice.

Dr. Morrison then asked the audience to offer their opinions on the best approach to diagnosing these neoplasms and whether adequate evidence exists in the literature to recommend changing the diagnosis from astrocytoma to another diagnostic term. Dr. Jerry Hardisty of EPL offered the most extensive comments. He stated that, in his opinion, using the term “astrocytoma” for these neoplasms should be avoided based on the current evidence and recommended using “glioma” when this neoplasm is encountered. However, if a treatment related increase is identified in a study, immunohistochemistry should be employed to determine the histogenesis since it could impact the assessment of human risk. Astrocytomas are a fairly common human neoplasm, but microglial tumors are very rare. In fact, microglial tumors do not commonly occur in any other species, suggesting that their occurrence in the rat could be a species-specific phenomenon, which would have obvious implications for risk assessment.

FINDINGS IN AN OCULAR STUDY

Dr. Cindy Farman of Genentech (South San Francisco, CA) and a member of the INHAND Special Senses OWG, presented lesions from a 14-day single-dose intravitreal (ITV) administration study in New Zealand white rabbits. The test material was administered bilaterally on day one. All eyes dosed with the test material developed mild to moderate inflammation, as detected on ophthalmic examination, starting at five days. There was no dose-severity response, and the controls were normal. At necropsy, on day 14, the eyes were collected, fixed in Davidson's solution, embedded in paraffin, and processed to H&E stained slides.

Light microscopic images (Figures 11A–F) were presented, with the following voting choices and results: endophthalmitis, mixed cellular (13%); infiltrate, mixed cellular, multifocal (5%); infiltrate, mononuclear cell, multifocal (4%); inflammation, mononuclear cell, multifocal (4%); panophthalmitis, mixed cellular (57%); and inflammation, mixed cellular, multifocal (17%). Thus, the majority consensus was that the ocular finding was mixed cellular panophthalmitis.

Cellular features of the finding included primarily mixed mononuclear cells, including plasma cells, with variable numbers of heterophils, affecting all layers and structures of the eye. Eosinophilic amorphous material, compatible with proteinaceous fluid, was present in the anterior and posterior compartments, and corneal edema was evident in some eyes. Although panophthalmitis would be an appropriate diagnosis based on traditionally accepted terminology for ocular pathology, inflammation, mixed cellular, would be the more appropriate diagnosis based on INHAND terminology guidelines.

Potential causes of the inflammation in this rabbit ocular study were discussed and included endotoxin contamination, injection-related sterile endophthalmitis, bacterial contamination, or test article-related. Endotoxin contamination typically has an onset within two days of test material administration. In these studies, endotoxin levels are always measured prior to ITV administration, and were within acceptable levels in this case. Injection-related sterile endophthalmitis is usually unilateral, typically occurs within two days of ITV administration, and is comprised of a mononuclear cell infiltrate. Bacterial contamination can occur due to either introduction of bacteria into a single eye as a result of the injection procedure (in which case it would be limited to single or sporadic eyes in a study) or contamination of the dose solution (and thus affecting a single or multiple groups); the infiltrate would usually be primarily heterophilic. Test materials for ITV studies are always evaluated for bacterial burden prior to injection and there was no bacterial burden detected in this test material. If dosing was bilateral, then test article-related inflammation would likely be bilateral and, depending on the situation, all dose groups may be affected. If there is an immune-mediated response to the test article, plasma cells may be a prominent component of the cellular infiltrate.

Dr. Farman informed the audience that the test material in this rabbit study was a humanized antibody product, and the inflammation was typical of an immune-mediated response to a foreign protein injected into the rabbit eye. The onset of the response at five days was earlier

than the “classically” expected 14 days, but all other features suggested an immune response. Rabbits are highly reactive to foreign proteins injected intravitreally, and this type of inflammatory response is very predictable in these rabbit studies. The same format injected into cynomolgus monkey eyes only resulted in minimal to mild infiltrates of mixed mononuclear inflammatory cells into various ocular structures, without additional indicators of inflammation such as edema or protein exudate. The test material in this study was originally designed by the protein engineering group in a manner to allow the most efficient large scale commercial production. However, it was re-engineered because of the inflammation in rabbits, and because pre-existing antibodies had been detected in monkeys. The new format, when tested in a single-dose study in rabbits, only caused minimal to mild mononuclear cell infiltrates without additional signs of inflammation such as protein exudate or edema.

Inflammation typical of an immune response occurs predictably upon intravitreal administration of antibody therapeutics to rabbits, and is especially severe after multiple doses. The inflammation always results in early termination of multi-dose rabbit studies, and can cause difficulty in interpreting whether there is specific test article toxicity underlying the inflammation. However, because of regulatory expectations for approval of this antibody product, a multi-dose rabbit IND-enabling study was conducted. The plan was for a three-month study, with dosing every two weeks (up to eight doses), with a one-month recovery and with three dose levels. As Dr. Farman and colleagues predicted, the study could not be carried to completion due to the development of extensive inflammation in the rabbit eyes. Thirteen of forty animals had to be euthanized early on days 15 and 43, and the remaining animals were euthanized on day 45. She concluded that, in her experience, multiple dose intravitreal studies with protein therapeutics in rabbits are not useful as part of nonclinical development programs.

AN UNUSUAL SPONTANEOUS OCULAR LESION IN A RAT

Dr. Leandro Teixeira of the University of Wisconsin-Madison and a member of the INHAND Special Senses OWG, presented an unusual spontaneous ocular lesion in a rat with challenging terminology. Significant contributions to this talk were made by Dr. Kohji Tanaka (Kobe Pharma Research Institute Nippon Boehringer Ingelheim Co., Kobe, Japan).

The lesion was seen in a routine ophthalmoscopic exam in a 12-week-old male, untreated control Sprague-Dawley rat and presented clinically as a unilateral focal posterior lenticular opacity in the right eye that was interpreted as retinal detachment. The audience was shown representative images (Figures 12A–D) and was asked to vote. The voting choices and answers were persistent hyperplastic primary vitreous [PHPV (22%)], persistent hyperplastic *tunica vasculosa lentis* [PHTVL (18%)], persistent hyperplastic primary vitreous and persistent hyperplastic *tunica vasculosa lentis* [PHPV/PHTVL (36%)], persistent fetal vasculature [PFV (12%)], multifocal retinal folds with epi-retinal membrane (6%), geographic retinal dysplasia with epi-retinal membrane (5%) and proliferative retinopathy (1%). The votes were evenly spread but the audience members’ first choice was PHPV/PHTVL. The contributor’s first choice was persistent fetal vasculature (PFV).

Dr. Teixeira then presented an overview of the hyaloid vascular system (HVS) in the developing mammalian eye. The HVS is a fetal ocular structure devoted to supply nutrients to the developing ocular tissues. It is composed of the hyaloid artery (a branch of the ophthalmic or central retinal artery) that branches anteriorly, forming the vasa hyaloidea propria (VHP) and the tunica vasculosa lentis (TVL) that surrounds the lens (Ito and Yoshioka 1999). These vessels normally regress late in human fetal development and in the first several weeks of life in most animal species (Goldberg 1997). A failure on the normal regression of these vessels gives rise to a developmental malformation called PHPV and/or PHTVL (Reese 1955). The degree of vascular regression will dictate the severity of the ocular lesions with the most prominent resulting in PHPV and PHTVL and the less prominent, sometimes non-clinical, resulting in persistent hyaloid artery and pre-retinal arterial loop (Shastry 2009). In order to more accurately reflect the broader manifestations of failed regression of the ocular vascular networks, Goldberg (1997) proposed a revision in the nomenclature, suggesting the term “persistent fetal vasculature” (PFV). PFV has been reported in humans (Reese, 1955; Goldberg, 1997), miniature schnauzer, basset hound, Siberian husky, beagle and Doberman dogs (Dubielzig et al. 2010), cats (Allgoewer and Pfefferkoprn 2001), Gottingen minipigs and Yucatan micropigs (Schafer and Render 2013), Sprague-Dawley rats (Kuno et al. 1991) and multiple transgenic mice including p53-null (Reichel et al. 1998), arf-null (Martin et al. 2004) and VEGF overexpressing (Taharaguchi et al. 2005) mice.

This brief discussion was followed by a description of the histological features of the different presentations of PFV. A persistent hyaloid artery is characterized by a small vessel extending from the optic disc surface into the vitreous. Similarly, a pre-retinal arteriolar loop implies an arteriole emerging from the central retinal artery, coursing through the posterior vitreous, and reconnecting to the inner retina (Tanaka et al. 1994). A PHTVL is characterized by small and regularly distributed vessels surrounding the posterior, equatorial and peripheral anterior lens capsule (Figure 12D). A PHPV is defined by a proliferation of vessels and fibroblasts forming an epi-retinal to retro-lenticular mass (Figures 12A and 12B), usually associated with posterior cortical cataract, intra-lenticular and vitreal hemorrhage, retinal detachment and/or folds (Figure 12C) and possibly by the presence of pigmented cells, glial cells, cartilage and adipose tissue admixed with the fibrovascular proliferation (Dubielzig et al. 2010).

After reviewing the background information and the microscopic features of the disease, Dr. Teixeira returned to the voting choices and discussed the answers. The diagnostic choices of PHPV, PHTVL and PHPV/PHTVL were correct in theory, but the contributors preferred the more inclusive diagnosis of PFV. Retinal folds were first reported in 1943 in Wistar rats (Poulsom and Hayes 1988) and usually represent a congenital lesion. Artifactual retinal folds (Lange’s folds) have been described in the peripheral retina of young animals and are associated with tissue fixation with 70% ethanol (Gartner and Henkind 1981). The term “retinal dysplasia” suggests a primary developmental retinal lesion characterized by focal to multifocal rosette-like and tubular structures expanding and distorting the inner and outer nuclear layers (Hubert et al. 1994). These two lesions are usually not accompanied by a vitreal fibrovascular proliferation. Finally, proliferative retinopathy is characterized by intra- and sub-retinal neovascular proliferation associated with diabetes and/or chronic

hyperglycemia (Mancini et al. 2013). Based on the few comments made during the final discussion, the audience agreed with the use of the “umbrella term” persistent fetal vasculature to describe this lesion.

Acknowledgments

The authors wish to thank Eli Ney of the NIEHS for her unique and creative cover artwork for the symposium handouts. Thanks also to Beth Mahler of EPL for her assistance with manuscript image preparation and for assistance during the symposium. The authors are grateful to Drs. Cynthia Willson and Erin Quist of the NIEHS for their critical review of this manuscript. Appreciation also goes to Maureen Kettering, Kim Brock, Tierre Miller and Matthew Price of Association Innovation and Management, Inc. for their valuable help with annual advertising and meeting facilities. Also integral to the success of this meeting was the audiovisual technical expertise provided by CMI Communications. Refreshments were graciously provided by Experimental Pathology Laboratories, Inc. and Charles River Laboratories, Inc.

This research was supported [in part] by the Intramural Research Program of the National Institutes of Health (NIH), National Institute of Environmental Health Sciences (NIEHS).

References

Abcam product description website. Anti-CD68 antibody [ED1] (ab31630). Retrieved November 22, 2015: http://www.abcam.com/cd68-antibody-ed1-ab31630.html

Adams ET, Auerbach S, Blackshear PE, Bradley A, Gruebbel MM, Little PB, Malarkey D, Maronpot R, McKay JS, Miller RA, Moore RR, Morrison JP, Nyska A, Ramot Y, Rao D, Suttie A, Wells MY, Willson GA, Elmore SA. Proceedings of the 2010 National Toxicology Program Satellite Symposium. Toxicol Pathol. 2011; 39:240–66. [PubMed: 21177527]

Adsay NV, Andea A, Basturk O, Kilinc N, Nassar H, Cheng JD. Secondary tumors of the pancreas: an analysis of a surgical and autopsy database and review of the literature. Virchows Arch. 2004; 444:527–35. [PubMed: 15057558]

Allgoewer I, Pfefferkorn B. Persistent hyperplastic tunica vasculosa lentis and persistent hyperplastic primary vitreous (PHTVL/PHPV) in two cats. Vet Ophthalmol. 2001; 4:161–4. [PubMed: 11423000]

American Cancer Society. Breast Cancer Overview [Internet]. Atlanta: American Cancer Society; c2014–15. [updated 2015 June 10; cited 2015 Nov 12]. Available at: http://www.cancer.org/Cancer/BreastCancer/OverviewGuide/breast-cancer-overview-key-statistics

Anderson N, Borlak J. Drug-induced phospholipidosis. FEBS Lett. 2006; 580:5533–40. [PubMed: 16979167]

Balbo S, James-Yi S, Johnson CS, O’Sullivan MG, Stepanov I, Wang M, Bandyopadhyay D, Kassie F, Carmella S, Upadhyaya P, Hecht SS. (S)-N′-Nitrosonornicotine, a constituent of smokeless tobacco, is a powerful oral cavity carcinogen in rats. Carcinogenesis. 2013; 34:2178–2183. [PubMed: 23671129]

Balbo S, Johnson CS, Kovi RC, James-Yi SA, O’Sullivan MG, Wang M, Le CT, Khariwala SS, Upadhyaya P, Hecht SS. Carcinogenicity and DNA adduct formation of 4-(methylnitrosamino)-1-(3-pyridyl)-1-butanone and enantiomers of its metabolite 4-(methylnitrosamino)-1-(3-pyridyl)-1-butanol in F-344 rats. Carcinogenesis. 2014; 35:2798–2806. [PubMed: 25269804]

Bach U, Hailey JR, Hill GD, Kaufmann W, Latimer KS, Malarkey DE, Maronpot RM, Miller RA, Moore RR, Morrison JP, Nolte T, Rinke M, Rittinghausen S, Suttie AW, Travlos GS, Vahle JL, Willson GA, Elmore SA. Proceedings of the 2009 National Toxicology Program Satellite Symposium. Toxicol Pathol. 2010; 38:9–36. [PubMed: 20008954]

Bern C. Chagas’ disease. N Engl J Med. 2015; 373:456–66. [PubMed: 26222561]

Block, D., Stevens, ED. Tuna: physiology, ecology, and evolution. Academic press; 2001. p. 468

Blomström AL, Widén F, Hammer AS, Belák S, Berg M. Detection of a novel astrovirus in brain tissue of mink suffering from shaking mink syndrome by use of viral metagenomics. J Clin Microbiol. 2010; 48:4392–4396. [PubMed: 20926705]

Boorman G, Crabbs TA, Kolenda-Roberts H, Latimer K, Miller AD, Muravnick KB, Nyska A, Ochoa R, Pardo ID, Ramot Y, Rao DB, Schuh J, Suttie A, Travlos GS, Ward JM, Wolf JC, Elmore SA. Proceedings of the 2011 National Toxicology Program Satellite Symposium. Toxicol Pathol. 2012; 40:321–44. [PubMed: 22089839]

Bourke CA. Cerebellar degeneration in goats grazing *Solanum cinereum* (Narrawa burr). Aust Vet J. 1997; 75:363–365. [PubMed: 9196830]

Bouzalas IG, Wüthrich D, Walland J, Drögemüller C, Zurbriggen A, Vandevelde M, Oevermann A, Bruggmann R, Seuberlich T. Neurotropic astrovirus in cattle with nonsuppurative encephalitis in Europe. J Clin Microbiol. 2014; 52:3318–3324. [PubMed: 24989603]

Braekevelt CR. Electron microscopic study of the occlusible tapetum lucidum of the southern fiddler ray (Trygonorhina fasciata). Histol Histopath. 1991; 6:509–514.

Brown JR, Morfopoulou S, Hubb J, Emmett WA, Ip W, Shah D, Brooks T, Paine SM, Anderson G, Virasami A, Tong CY, Clark DA, Plagnol V, Jacques TS, Qasim W, Hubank M, Breuer J. Astrovirus VA1/HMO-C: an increasingly recognized neurotropic pathogen in immunocompromised patients. Clin Infect Dis. 2015; 60:881–888. [PubMed: 25572899]

Cammer W. Glutamine synthetase in the central nervous system is not confined to astrocytes. J Neuroimmunol. 1990; 26:173–178. [PubMed: 1688879]

Campidelli C, Agostinelli C, Stitson R, Pileri SA. Myeloid sarcoma extramedullary manifestation of myeloid disorders. Am J Clin Pathol. 2009; 132:426–437. [PubMed: 19687319]

Carey FG. Bluefin tuna warm their viscera during digestion. J exp bio. 1984; 109:1–20.

Cartwright ME, Petruska J, Arezzo J, Frank D, Litwak M, Morrissey RE, MacDonald J, Davis TE. Phospholipidosis in neurons caused by posaconazole, without evidence for functional neurologic effects. Toxicol Pathol. 2009; 37:902–10. [PubMed: 19833913]

Cech JJ, Laurs RM, Graham JB. Temperature induced changes in blood gas equilibria in the Albacore, a warm-blooded Tuna. J exp Biol. 1984; 109:21–34.

Chandler, FW., Watts, JC. Pathologic Diagnosis of Fungal Infections. 1987. p. 123-125.p. 204

Chang JC, Ciaccio P, Schroeder P, Wright L, Westwood R, Berg AL. Pathology and Neurotoxicity in Dogs after Repeat Dose Exposure to a Serotonin 5-HT1B Inhibitor. J Toxicol Pathol. 2014; 27:31–42. [PubMed: 24791065]

Chanut F, Kimbrough C, Hailey R, Berridge B, Hughes-Earle A, Davies R, Roland K, Stokes A, Casartelli A, York M, Jordan H, Crivellente F, Cristofori P, Thomas H, Klapwijk J, Adler R. Spontaneous cardiomyopathy in young Sprague-Dawley rats: evaluation of biological and environmental variability. Toxicol Pathol. 2013; 41:1126–36. [PubMed: 23475560]

Cross, PC., Mercer, KL. Cell and Tissue Ultrastructure: A Functional Perspective. W.H. Freeman and Company; New York: 2002. p. 310-316.

Damoiseaux JG, Dopp EA, Calame W, Chao D, MacPherson GG, Dijkstra CD. Rat macrophage lysosomal membrane antigen recognized by monoclonal antibody ED1. Immunology. 1994; 83:140–7. [PubMed: 7821959]

Davis, B., Fenton, S. Mammary Gland. In: Hascheck, WM.Rousseaux, CG., Wallig, MA., editors. Hascheck and Rousseaux's Handbook of Toxicologic Pathology. Third. Elsevier; Oxford, UK: 2013. p. 2665-2691.

De Barros SS, Riet-Correa F, Andujar MB, Lombardo de Barros CS, Méndez MC, Schild AL. *Solanum fastigiatum* var. Fastigiatum and *Solanum* sp. poisoning in cattle: ultrastructural changes in the cerebellum. Pesquisa Veterinária Brasileira. 1987; 7:1–5.

Delclos KB, Camacho L, Lewis SM, Vanlandingham MM, Latendresse JR, Olson GR, Davis KJ, Patton RE, Gamboa da Costa G, Woodling KA, Bryant MS, Chidambaram M, Trbojevich R, Juliar BE, Felton RP, Thorn BT. Toxicity evaluation of bisphenol A administered by gavage to Sprague Dawley rats from gestation day 6 through postnatal day 90. Toxicol Sci. 2014; 139:174–97. [PubMed: 24496637]

Dubielzig, R.Ketring, K.McLellan, GJ., Albert, DM., editors. Veterinary Ocular Pathology: A Comparative Review. Saunders Elsevier; Edinburgh, UK: 2010. The retina; p. 350-53.p. 356

Dumont JN. Prolactin-induced cytologic changes in the mucosa of the pigeon crop during crop- "milk" formation. Z Zellforsch Mikrosk Anat. 1965; 68:755–82. [PubMed: 5877243]

Elmore SA, Berridge BR, Boyle MC, Cora MC, Hoenerhoff MJ, Kooistra L, Laast VA, Morrison JP, Rao D, Rinke M, Yoshizawa K. Proceedings of the 2012 National Toxicology Program Satellite Symposium. Toxicol Pathol. 2013; 41:151–80. [PubMed: 23262640]

Elmore SA, Boyle MC, Boyle MH, Cora MC, Crabbs TA, Cummings CA, Gruebbel MM, Johnson CL, Malarkey DE, McInnes EF, Nolte T, Shackelford CC, Ward JM. Proceedings of the 2013 National Toxicology Program Satellite Symposium. Toxicol Pathol. 2014; 42:12–44. [PubMed: 24334674]

Elmore SA, Cora MC, Gruebbel MM, Hayes SA, Hoane JS, Koizumi H, Peters R, Rosol TJ, Singh BP, Szabo KA. Proceedings of the 2014 National Toxicology Program Satellite Symposium. Toxicol Pathol. 2015; 43:10–40. [PubMed: 25385331]

Esch KJ, Peterson CA. Transmission and epidemiology of zoonotic protozoal diseases of companion animals. Clin Microbiol Rev. 2013; 26:58–85. [PubMed: 23297259]

Ettlin RA, Kuroda J, Plassmann S, Hayashi M, Prentice DE. Successful drug development despite adverse preclinical findings part 2: examples. J Toxicol Pathol. 2010; 23:213–34. [PubMed: 22272032]

Eustis, et al. Liver. In: Boorman, et al., editors. Pathology of the Fischer Rat. Academic Press; 1990. p. 74

Figarella-Branger D, Dufour H, Fernandez C, Bouvier-Labit C, Grisoli F, Pellissier JF. Pituicytomas, a mis-diagnosed benign tumor of the neurohypophysis: report of three cases. Acta Neuropathol. 2002; 104:313–9. [PubMed: 12172918]

Figarella-Branger, D., Soylemezoglu, F., Kleihues, P., Hassoun, J. Central Neurocytoma. In: Kleihues, P., Cavenee, WK., editors. WHO Classification of Tumours of the Nervous System. IARC Press; Lyon, France: 2000. p. 107-109.

Fudge DS, Stevens ED. The visceral retia mirabilia of tuna and sharks: an annotated translation and discussion of the Eschricht and Muller 1835 paper and related papers. Guelph Ichthyology Reviews. 1996 Feb.(4):1–92.

Gartner S, Henkind P. Lange's folds: a meaningful ocular artifact. Ophthalmology. 1981; 88:1307–1310. [PubMed: 7322481]

Gildea LA, Morris RE, Newman SL. *Histoplasma capsulatum* yeasts are phagocytized via very late antigen-5, killed, processed for antigen presentation by human dendritic cells. J Immunol. 2001; 166:1049–1056. [PubMed: 11145684]

Gillespie MJ, Haring VR, McColl KA, Monaghan P, Donald JA, Nicholas KR, Moore RJ, Crowley TM. Histological and global gene expression analysis of the 'lactating' pigeon crop. BMC Genomics. 2011; 12:452. [PubMed: 21929790]

Gillespie MJ, Crowley TM, Haring VR, Wilson SL, Harper JA, Payne JS, Green D, Monaghan P, Stanley D, Donald JA, Nicholas KR, Moore RJ. Transcriptome analysis of pigeon milk production - role of cornification and triglyceride synthesis genes. BMC Genomics. 2013; 14:169. [PubMed: 23497009]

Goldberg M. Persistent fetal vasculature (PFV): an integrated interpretation of signs and symptoms associated with persistent hyperplastic primary vitreous (PHPV) LIV Edward Jackson Memorial Lecture. Am J Ophthalmol. 1997; 124:587–626. [PubMed: 9372715]

Greaves, P. Histopathology of Preclinical Toxicity Studies; Interpretation and Relevance in Drug Safety Evaluation. 2nd. Elsevier Sciences B.B; Amsterdam, The Netherlands: 2000. Cardiovascular System; Heart and Pericardium; p. 254-278.

Guaraná ELS, Riet-Correa F, Mendonça CL, Medeiros RMT, Costa NA, Afonso JAB. Intoxicação por *Solanum paniculatum* (Solanaceae) em bovinos. Pesqui Vet Bras. 2011; 31:59–64.

Halliwell WH. Cationic amphiphilic drug-induced phospholipidosis. Toxicol Pathol. 1997; 25:53–60. [PubMed: 9061852]

Hachem S, Aguirre A, Vives V, Marks A, Gallo V, Legraverend C. Spatial and temporal expression of S100B in cells of oligodendrocyte lineage. Glia. 2005 Aug 1; 51(2):81–97. [PubMed: 15782413]

Hatton GI. Pituicytes, glia and control of terminal secretion. J Exp Biol. 1988; 139:67–79. [PubMed: 3062122]

Hecht SS. Biochemistry, biology, and carcinogenicity of tobacco-specific N-nitrosamines. Chem Res Toxicol. 1998; 11:559–603. [PubMed: 9625726]

Hegde SN. Composition of pigeon milk and its effect on growth in chicks. Indian J Exp Biol. 1972; 11:238–239.

HogenEsch H, Broerse JJ, Zurcher C. Neurohypophyseal astrocytoma (Pituicytoma) in a rhesus monkey (Macaca mulatta). Vet Pathol. 1992 Jul; 29(4):359–61. [PubMed: 1514223]

Howlader, N.Noone, AM.Krapcho, M.Garshell, J.Miller, D.Altekruse, SF.Kosary, CL.Yu, M.Ruhl, J.Tatalovich, Z.Mariotto, A.Lewis, DR.Chen, HS.Feuer, EJ., Cronin, KA., editors. SEER Cancer Statistics Review, 1975–2012 [Internet]. Bethesda (MD): National Cancer Institute; c2014–15. [updated 2015 Aug 20; cited 201 Nov 12]. Available at: http://seer.cancer.gov/csr/1975_2012/

Hubert MF, Gillet JP, Durand-Cavagna G. Spontaneous retinal changes in Sprague Dawley rats. Lab Anim Sci. 1994; 44:561–7. [PubMed: 7898028]

Huisinga M, Henrich M, Frese K, Burkhardt E, Kuchelmeister K, Schmidt M, Reinacher M. Extraventricular neurocytoma of the spinal cord in a dog. Vet Pathol. 2008 Jan; 45(1):63–6. [PubMed: 18192579]

Interagency Breast Cancer and the Environment Research Coordinating Committee (IBCERCC). Department of Health and Human Services. Breast Cancer and the Environment: Prioritizing Prevention. 2013. Available at: https://www.niehs.nih.gov/about/assets/docs/breast_cancer_and_the_environment_prioritizing_prevention_508.pdf

Ito D, Imai Y, Ohsawa K, Nakajima K, Fukuuchi Y, Kohsaka S. Microglia-specific localisation of a novel calcium binding protein, Iba1. Brain Res Mol Brain Res. 1998 Jun 1; 57(1):1–9. [PubMed: 9630473]

Ito M, Yoshioka M. Regression of the hyaloid vessels and pupillary membrane of the mouse. Anat Embryol. 1999; 200:403–11. [PubMed: 10460477]

Iyonaga K, Takeya M, Yamamoto T, Ando M, Takahashi K. A novel monoclonal antibody, RM-4, specifically recognizes rat macrophages and dendritic cells in formalin-fixed paraffin-embedded tissues. Histochem J. 1997 Feb; 29(2):105–16. [PubMed: 9147067]

Jokinen MP, Lieuallen WG, Boyle MC, Johnson CL, Malarkey DE, Nyska A. Morphologic aspects fo rodent cardiotoxicity in a retrospective evaluation of National Toxicology Program studies. Toxicologic Pathology. 2011; 39:850–860. [PubMed: 21747121]

Kolenda-Roberts HM, Harris N, Singletary E, Hardisty JF. Immunohistochemical characterization of spontaneous and acrylonitrile-induced brain tumors in the rat. Toxicol Pathol. 2013 Jan; 41(1):98–108. [PubMed: 22821367]

Krinke GJ, Kaufmann W, Mahrous AT, Schaetti P. Morphologic characterization of spontaneous nervous system tumors in mice and rats. Toxicol Pathol. 2000 Jan-Feb;28(1):178–92. [PubMed: 10669006]

Kuno H, Usui T, Eydelloth RS, Wolf ED. Spontaneous ophthalmic lesions in young Sprague-Dawley rats. J Vet Med Sci. 1991; 53:607–614. [PubMed: 1834202]

LaFountain AM, Prum RO, Frank HA. Diversity, physiology, and evolution of avian plumage carotenoids and the role of carotenoid-protein interactions in plumage color appearance. Arch Biochem Biophys. 2015 Apr 15.572:201–12. [PubMed: 25637658]

Li L, Diab S, McGraw S, Barr B, Traslavina R, Higgins R, Talbot T, Blanchard P, Rimoldi G, Fahsbender E, Page B, Phan TG, Wang C, Deng X, Pesavento P, Delwart E. Divergent astrovirus associated with neurologic disease in cattle. Emerg Infect Dis. 2013; 19:1385–1392. [PubMed: 23965613]

Lima EF, Riet-Correa F, Trindade de Medeiros RM. Spontaneous poisoning by *Solanum subinerme* Jack as a cause of cerebellar cortical degeneration in cattle. Toxicon. 2014; 82:93–96. [PubMed: 24561122]

Mancini JE, Croxatto JO, Gallo JE. Proliferative retinopathy and neovascularization of the anterior segment in female type 2 diabetic rats. Diabetology & Metabolic Syndrome. 2013; 5:68. [PubMed: 24499599]

Martin AC, Thornton JD, Liu J, Wang X, Zuo J, Jablonski MM, Chaum E, Zindy F, Skapek SX. Pathogenesis of persistent hyperplastic primary vitreous in mice lacking the arf tumor suppressor gene. Invest Ophthalmol Vis Sci. 2004; 45:3387–96. [PubMed: 15452040]

Menzies JS, Bridges CH, Bailey EM. A neurological disease of cattle associated with *Solanum dimidiatum*. Southwest Veterinary. 1979; 32:45–49.

Moroki T, Sasaki T, Yoshizawa K, Doi T. A spontaneously occurring malignant pituicytoma in a male sprague dawley rat. J Toxicol Pathol. 2015 Jul; 28(3):171–6. [PubMed: 26441479]

Moser LA, Schultz-Cherry S. Pathogenesis of astrovirus infection. Viral Immunol. 2005; 18:4–10. [PubMed: 15802949]

Nagatani M, Ando R, Yamakawa S, Saito T, Tamura K. Histological and immunohistochemical studies on spontaneous rat astrocytomas and malignant reticulosis. Toxicol Pathol. 2009 Aug; 37(5):599–605. [PubMed: 19487256]

Nakamura R, Nishimura T, Ochiai T, Nakada S, Nagatani M, Ogasawara H. Availability of a microglia and macrophage marker, iba-1, for differential diagnosis of spontaneous malignant reticuloses from astrocytomas in rats. J Toxicol Pathol. 2013 Mar; 26(1):55–60. [PubMed: 23723569]

Newman SL. Macrophages in host defense against *Histoplasma capsulatum*. Trends Microbiol. 1999; 7:67–71. [PubMed: 10081083]

Pace DM, Landolt PA, Mussehl FE. The effect of pigeon crop-milk on growth in chickens. Growth. 1952 Dec; 16(4):279–85. 1952. [PubMed: 13021575]

Park, YW., Haelnein, FW. Handbook of milk of non-bovine mammals. First. Blackwell Publishing; Oxford, UK: 2006.

Plante, I., Stewart, MK., Laird, DW. Evaluation of Mammary Gland Development and Function in Mouse Models; JoVE. 2011. p. 53Available at: http://www.jove.com/details.php?id=2828

Porta A, Maresca B. Host response and *Histoplasma capsulatum* / macrophage molecular interactions. Med Mycol. 2000; 38:399–406. [PubMed: 11204877]

Porter MB, MacKay RJ, Uhl E, Platt SR, de Lahunta A. Neurologic disease putatively associated with ingestion of *Solanum viarum* in goats. J Am Vet Med Assoc. 2003; 223:501–504. [PubMed: 12930090]

Poulsom R, Hayes B. Congenital retinal folds in Sheffield-Wistar rats. Graefes Arch Clin Exp Ophthalmol. 1988; 226:31–3. [PubMed: 3342972]

Prum RO, Torres R. Structural colouration of avian skin: convergent evolution of coherently scattering dermal collagen arrays. The Journal of Experimental Biology. 2003; 206:2409–2429. [PubMed: 12796458]

Prum RO, Torres RH. Structural colouration of mammalian skin: convergent evolution of coherently scattering dermal collagen arrays. J Exp Biol. 2004 May; 207(Pt 12):2157–72. [PubMed: 15143148]

Prum RO, Torres R, Kovach C, Williamson S, Goodman SM. Coherent light scattering by nanostructured collagen arrays in the caruncles of the malagasy asities (Eurylaimidae: aves). J Exp Biol. 1999 Dec; 202(Pt 24):3507–22. [PubMed: 10574729]

Reasor MJ, Hastings KL, Ulrich RG. Drug-induced phospholipidosis: issues and future directions. Expert Opin Drug Saf. 2006; 5:567–83. [PubMed: 16774494]

Reese A. Persistent hyperplastic primary vitreous. Am J Ophthalmol. 1955; 40:317–331. [PubMed: 13248898]

Reichel MB, Ali RR, D'Esposito F. High frequency of persistent hyperplastic primary vitreous and cataracts in p-53 deficient mice. Cell Death Differ. 1998; 5:156–62. [PubMed: 10200460]

Renne, R (Chair), Brix, A., Harkema, J., Herbert, R., Kittel, B., Lewis, D., March, T., Nagano, K., Pino, M., Rittinghausen, S., Rosenbruch, M., Tellier, P., Wohrmann, T. Proliferative and nonproliferative lesions of the rat and mouse respiratory tract. Toxicol Pathol. 2009; 37:5S–73S. [PubMed: 20032296]

Engberg, Ricarda M., Kaspers, B., Schranner, Iris, Koesters, J., Loesch, U. Quantification of the immunoglobulin classes IgG and IgA in the young and adult pigeon (Columba livia). Avian Pathology. 1992; 21:3, 409–420. [PubMed: 18670912]

Rivenson A, Hoffmann D, Prokopczyk B, Amin S, Hecht SS. Induction of lung and exocrine pancreas tumors in F344 rats by tobacco-specific and Areca-derived N-nitrosamines. Cancer Res. 1988; 48:6912–6917. [PubMed: 3180100]

Rodriguez FJ, Giannini C. Oligodendroglial tumors: diagnostic and molecular pathology. Semin Diagn Pathol. 2010 May; 27(2):136–45. [PubMed: 20860317]

Rossmeisl JH Jr, Piñeyro P, Sponenberg DP, Garman RH, Jortner BS. Clinicopathologic features of intracranial central neurocytomas in 2 dogs. J Vet Intern Med. 2012 Jan-Feb;26(1):186–91. [PubMed: 22233345]

Satoh H, Iwata H, Furuhama K, Enomoto M. Pituicytoma: primary astrocytic tumor of the pars nervosa in aging Fischer 344 rats. Toxicol Pathol. 2000 Nov-Dec;28(6):836–8. [PubMed: 11127300]

Schafer, KA., Render, JA. Toxicologic Pathology of the Eye: Alterations of the Lens and Posterior Segment. In: Weir, A., Collins, M., editors. Assessing Ocular Toxicology in Laboratory Animals. 1st. Humana Press; New York, NY: 2013. p. 219-257.

Schmidt-Nielsen, K. Animal Physiology: Adaptation and Environment. 2nd. Cambridge: Cambridge University Press; 1979.

Schmitz G, Müller G. Structure and function of lamellar bodies, lipid-protein complexes involved in storage and secretion of cellular lipids. J Lipid Res. 1991; 32:1539–1570. [PubMed: 1797938]

Shastry BS. Persistent hyperplastic primary vitreous: congenital malformation of the eye. Clin Exp Ophth. 2009; 37:884–90.

Showalter SL, Hager E, Yeo CJ. Metastatic disease to the pancreas and spleen. Semin Oncol. 2008; 35:160–171. [PubMed: 18396201]

Silver R. Prolactin and parenting in the Pigeon family. The Journal of Experimental Zoology. 1984; 232:617–625. [PubMed: 6394702]

Studer-Thiersch A. Füttern die Flamingos ihre Jungen mit Blut? (Do flamingos feed their chicks with blood?). Zolli-Bulletin Nr. 1963; 10:10–12.

Summers, BA., Cummings, JF., deLahunta, A. Principles of Neuropathology. In: Summers, B.Cummings, J., deLahunta, A., editors. Veterinary Neuropathology. Mosby Year Book, Inc; St. Louis, Missouri, USA: 1995. p. 10

Suzuki H, Franz H, Yamamoto T, Iwasaki Y, Konno H. Identification of the normal population in human and rodent nervous tissue using lectin-histochemistry. Neuropathol Appl Neurobiol. 1988 May-Jun;14(3):221–7. [PubMed: 3405394]

Tekeli S, Morton D, Cusick PK. Pituicytoma in a mouse. Toxicol Pathol. 1997 Sep-Oct;25(5):516–7. [PubMed: 9323844]

Taharaguchi S, Yoshida K, Tomioka Y, Yoshino S, Uede T, Ono E. Persistent hyperplastic primary vitreous in transgenic mice expressing IE 180 of the pseudorabies virus. Invest Ophthalmol Vis Sci. 2005; 46:1551–6. [PubMed: 15851549]

Tanaka K, Inagaki S, Doi K. Preretinal arteriolar loops in rats. Lab Anim Sci. 1994; 44:71–72. [PubMed: 8007666]

Thind SK, Taborda CP, Nosanchuk JD. Dendritic cell interactions with *Histoplasma* and *Paracoccidioides*. Virulence. 2015; 6:424–432. [PubMed: 25933034]

Tizard I. The avian antibody response. Semin Avian Exot Pet. 2002; 11:2–14.

van der Lugt JJ, Bastianello SS, van Ederen AM, van Wilpe E. Cerebellar cortical degeneration in cattle caused by *Solanum kwebense*. Vet J. 2010; 185:225–227. [PubMed: 19457687]

Verdes JM, Márquez M, Calliari A, Battes D, Moraña JA, Gimeno EJ, Odriozola E, Giannitti F, Guerrero F, Fidalgo LE, Pumarola M. A novel pathogenic mechanism for cerebellar lesions produced by *Solanum bonariense* in cattle. J Vet Diagn Invest. 2015; 27:278–286. [PubMed: 25901005]

Wang DD, Bordey A. The astrocyte odyssey. Prog Neurobiol. 2008 Dec 11; 86(4):342–67. [PubMed: 18948166]

Weber K, Garman RH, Germann PG, Hardisty JF, Krinke G, Millar P, Pardo ID. Classification of neural tumors in laboratory rodents, emphasizing the rat. Toxicol Pathol. 2011 Jan; 39(1):129–51. [PubMed: 21196527]

Bosman, FT.Carneiro, F.Hruban, RH., Theise, ND., editors. WHO classification of tumours of the digestive system. fourth. Vol. 3. IARC; 2010.

Williams GD. Naturally occurring trypanosomiasis (Chagas' disease) in dogs. J Am Vet Med Assoc. 1977; 171:171–177. [PubMed: 407202]

Young, B., Heath, JW. Wheater's Functional Histology: A Text and Colour Atlas. Churchill Livingstone; Edinburgh: 2000. p. 232p. 235

Zaki F, Harris J, Budzilovich G. Cystic pituicytoma of the neurohypophysis in a Siamese cat. J Comp Pathol. 1975 Jul; 85(3):467–71. [PubMed: 1141475]

Zhou Q, Wang S, Anderson DJ. Identification of a novel family of oligodendrocyte lineage-specific basic helix-loop-helix transcription factors. Neuron. 2000 Feb; 25(2):331–43. [PubMed: 10719889]

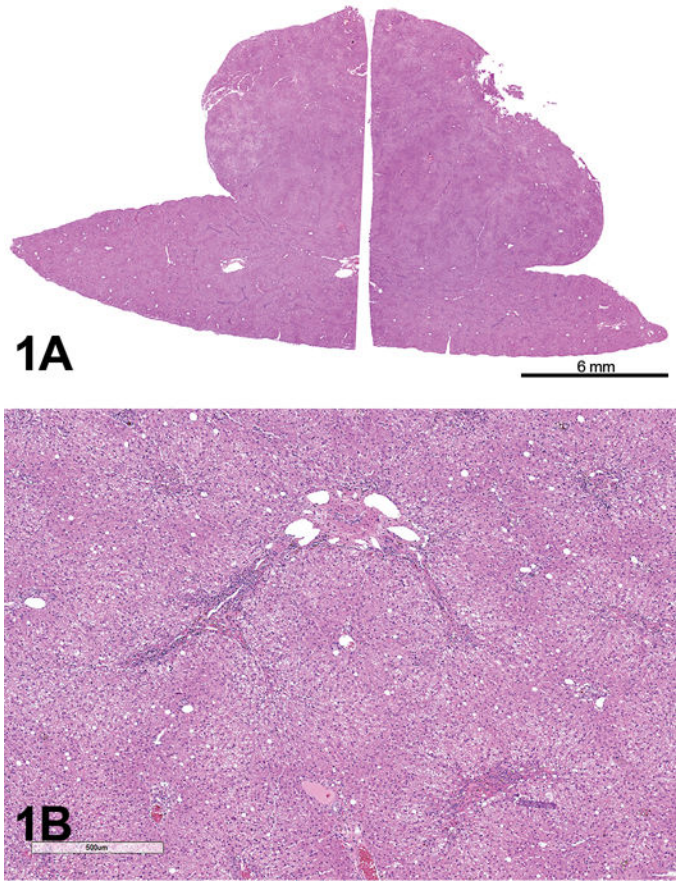

Figure 1.

(A–B). Benign nodular lesion of hepatocytes in the dog. Photomicrograph of a cross section of a liver mass on the left liver lobe of a dog (A) and a higher magnification photomicrograph of the mass in figure 1A (B), demonstrating portal tracts and distorted lobules accentuated by minimal portal bridging inflammation, fibrosis, and biliary hyperplasia. H&E.

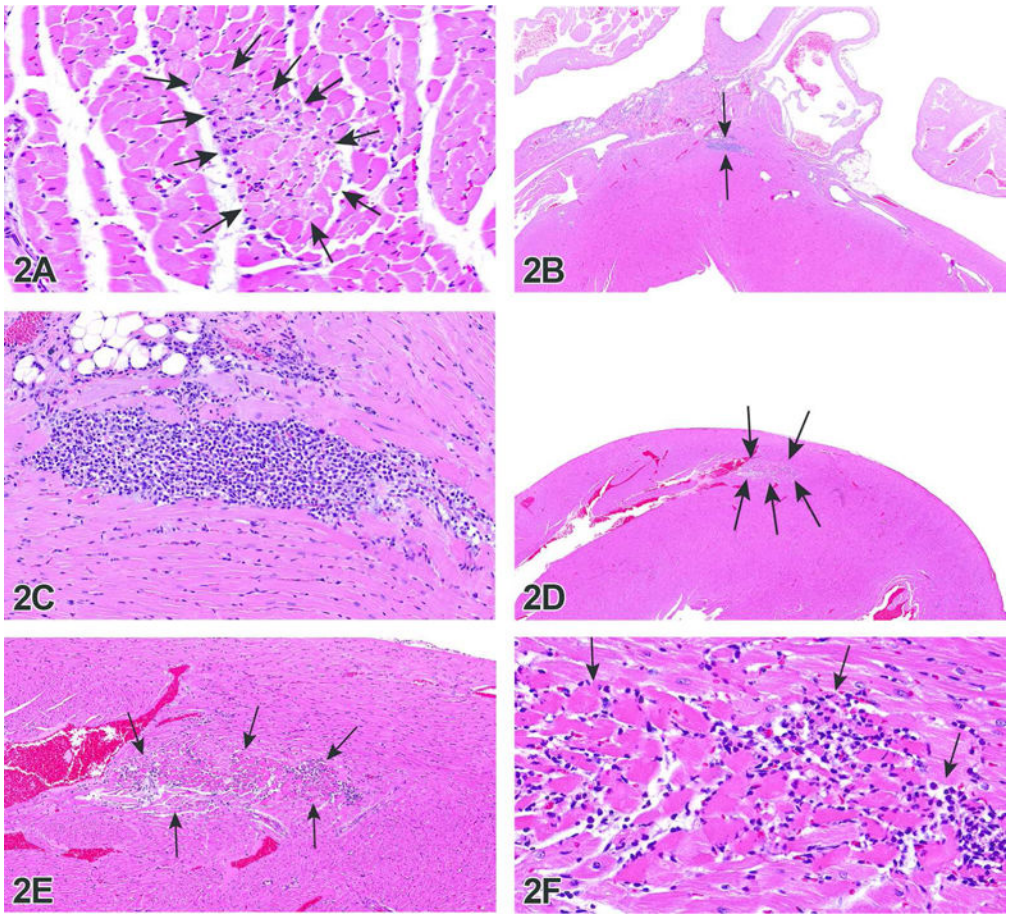

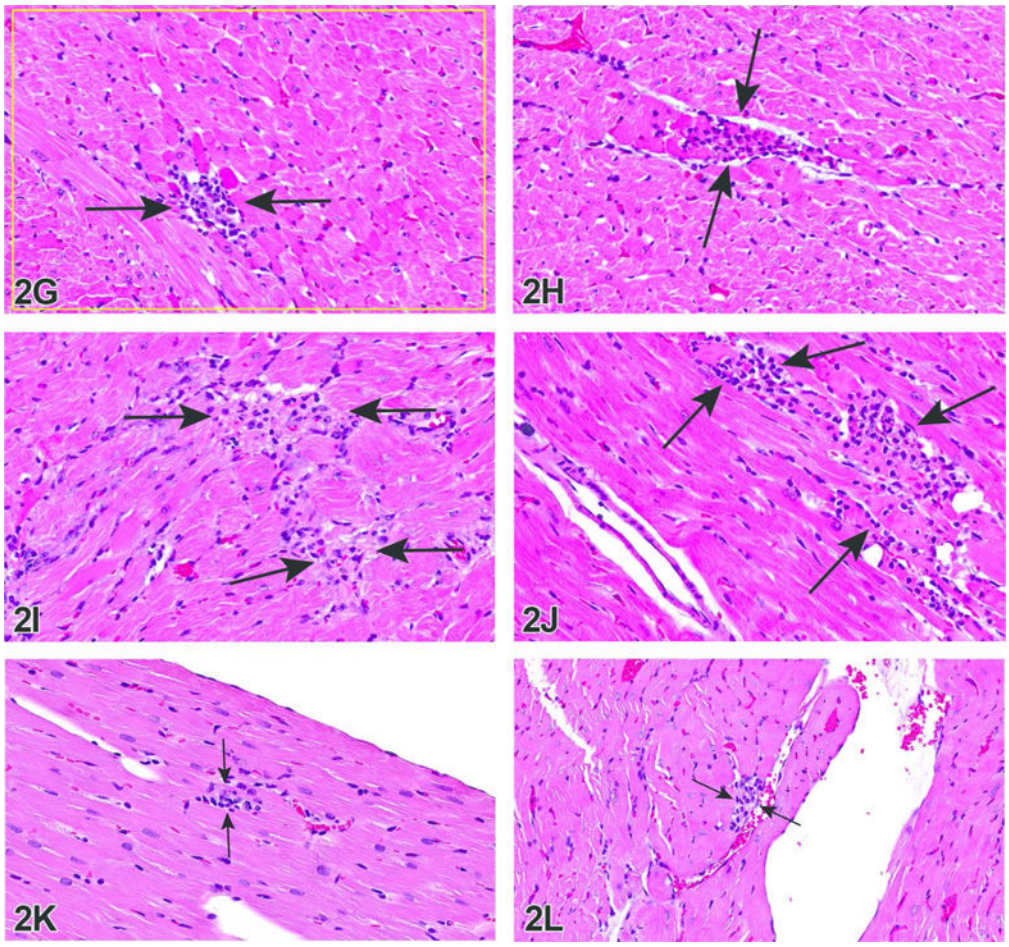

Figure 2.

(A–F). Heart lesions representing the spectrum of morphologies comprising cardiomyopathy in control male SD rats. Case 1 (A)-high magnification of a predominantly necrotic lesion within the left ventricle. Case 2 (B)-low magnification of a predominantly cellular lesion within the base of the heart and (C) high magnification. Case 3 (D)-low magnification of a mixed necrotic and cellular lesion within the apex of the heart, (E) mid magnification and (F) high magnification. H&E.

(G–L). Case 4 (G, H, I, J)-high magnifications of 4 lesions within the same heart (apex, right ventricle, left ventricle and septum). Case 5 (K)-high magnification of an “equivocal” lesion within the right ventricle. Case 6 (L)-high magnification of clear but very small lesion within the left ventricle. H&E.

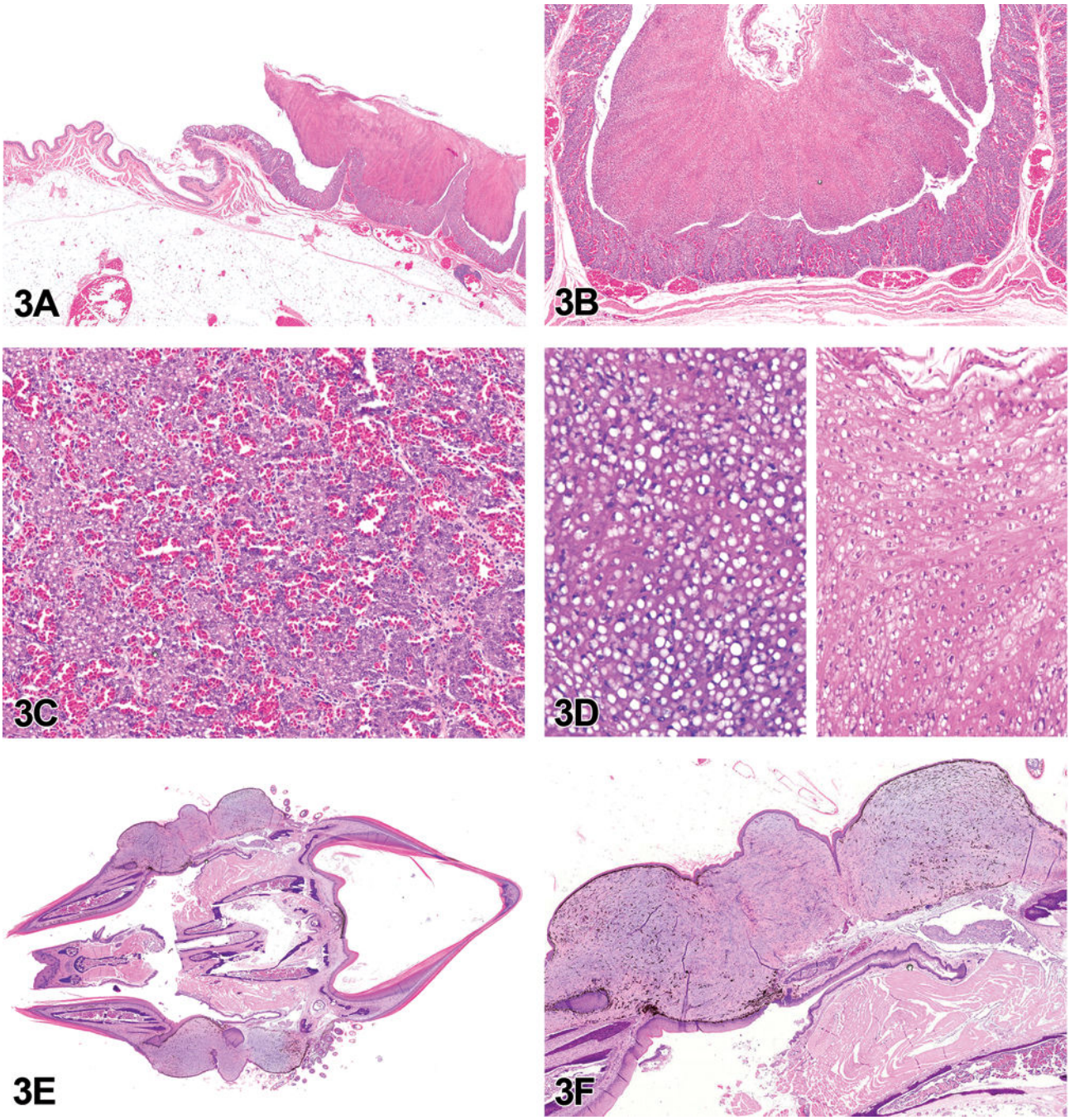

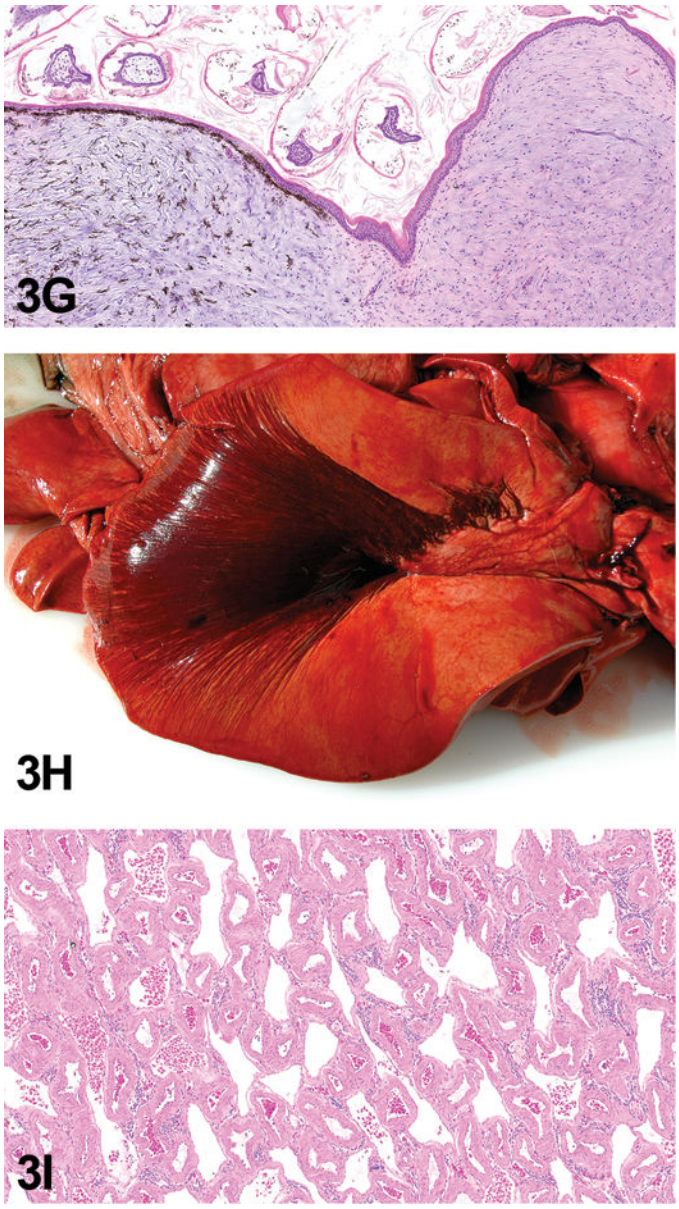

Figure 3.

(A–F). Various tissues from a Rock dove, a Gouldian finch and a tuna. (A) Esophagus (left) extending into crop (right), Rock dove (pigeon). There is massive hyperplasia (A) of the surface epithelium. (B) The basilar layers of the epithelial surface have massive interdigitated infoldings of a (C) highly vascularized subepithelial stroma. (D) The surface is a thick layer of epithelial cells that contain heavy concentrations of lipid (clear vacuoles) and protein (eosinophilia, hyperkeratosis). (E) The oral maxillary and mandibular surfaces of a young (nestling) Gouldian finch. (F) There are symmetric fibrous nodules at the commissures of the beak, one side of which is shown. The nodules are composed of organized collagen fibers, two of which (outer, grossly blue) have melanocytes interspersed with the stroma. H&E.

(G–I). The central nodule (G) is grossly yellow, with arrayed collagen similar to a fibrous tapetum. Scattered light through the fibrous arrays produce the blue and yellow colors seen grossly (http://www.aqua.org/explore/animals/gouldian-finch, accessed 11/30/15). Gross image (H) of the liver from a tuna. The visceral rete (I) is formed by massive branching of the celiac artery into parallel arteries that interdigitate with veins. The arteries and veins are closely apposed to cool cardiac arterial blood and warm visceral venous blood. Histology images are H&E.

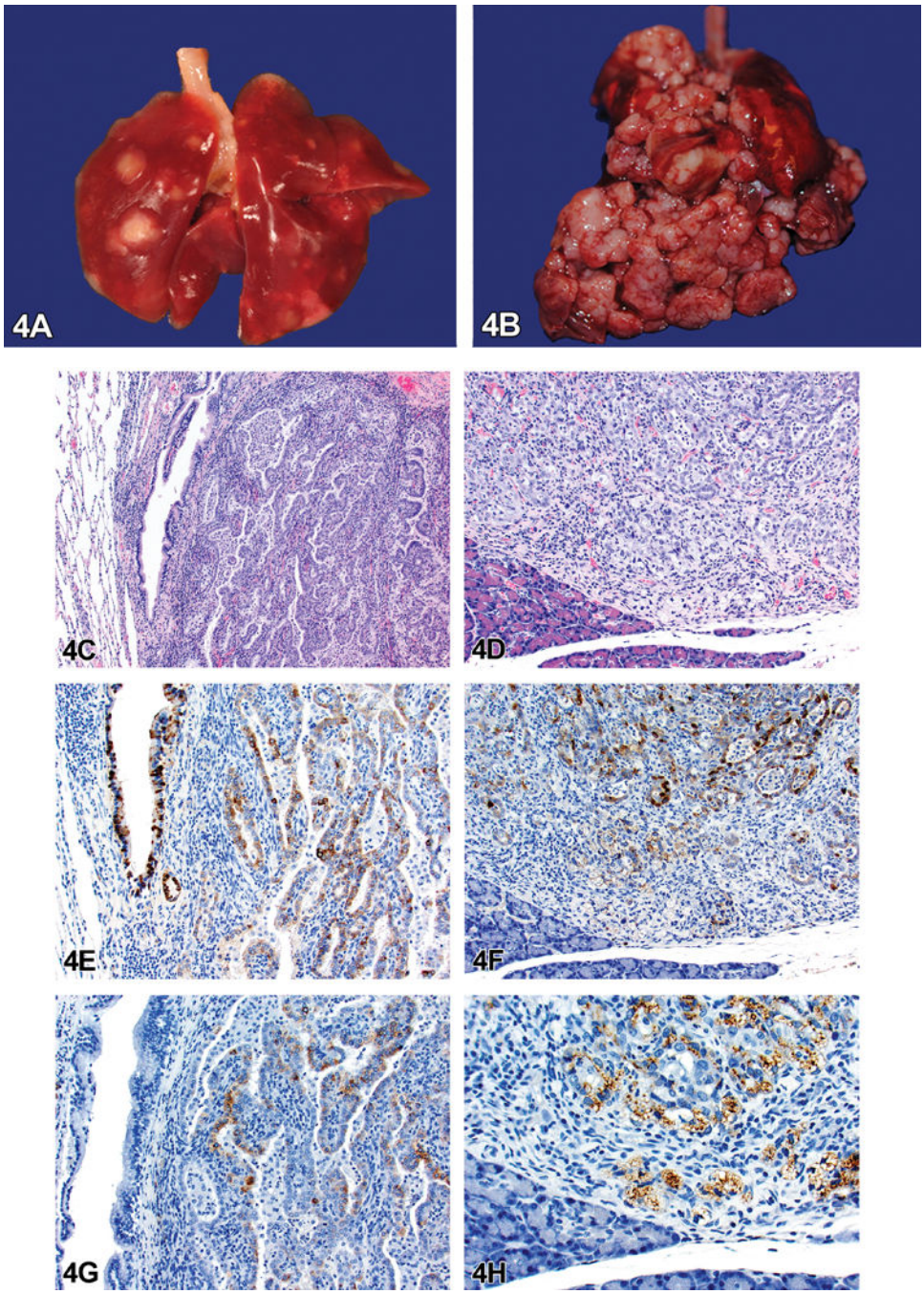

Figure 4.

(A–B). Alveolar/bronchiolar carcinoma with metastasis to the pancreas in male F344 rats from a 2-year carcinogenicity bioassay. Gross images of multifocal lung tumors from a rat treated with (*R*)-NNAL (A*), lung tumors with extrapulmonary masses invading the mediastinum and thoracic cavity (B*).

(C–H). Histomicrographs of alveolar/bronchiolar carcinoma from a rat treated with racemic NNAL. The microscopic lesion within the pancreas that was presented for voting (C) depicts an epithelial neoplastic mass that effaces the normal pancreatic architecture with

tubuloacinar structure formation (D) (H&E). Immunohistochemistry for alveolar type II cell marker, prosurfactant protein C (PSP-C) in lung tumor (E), and metastatic carcinoma in the pancreas (F); for Clara (club) cell marker CC10 in lung tumor (G) and metastatic carcinoma in the pancreas (H).

*Reproduced with permission from Balbo et al., 2014.

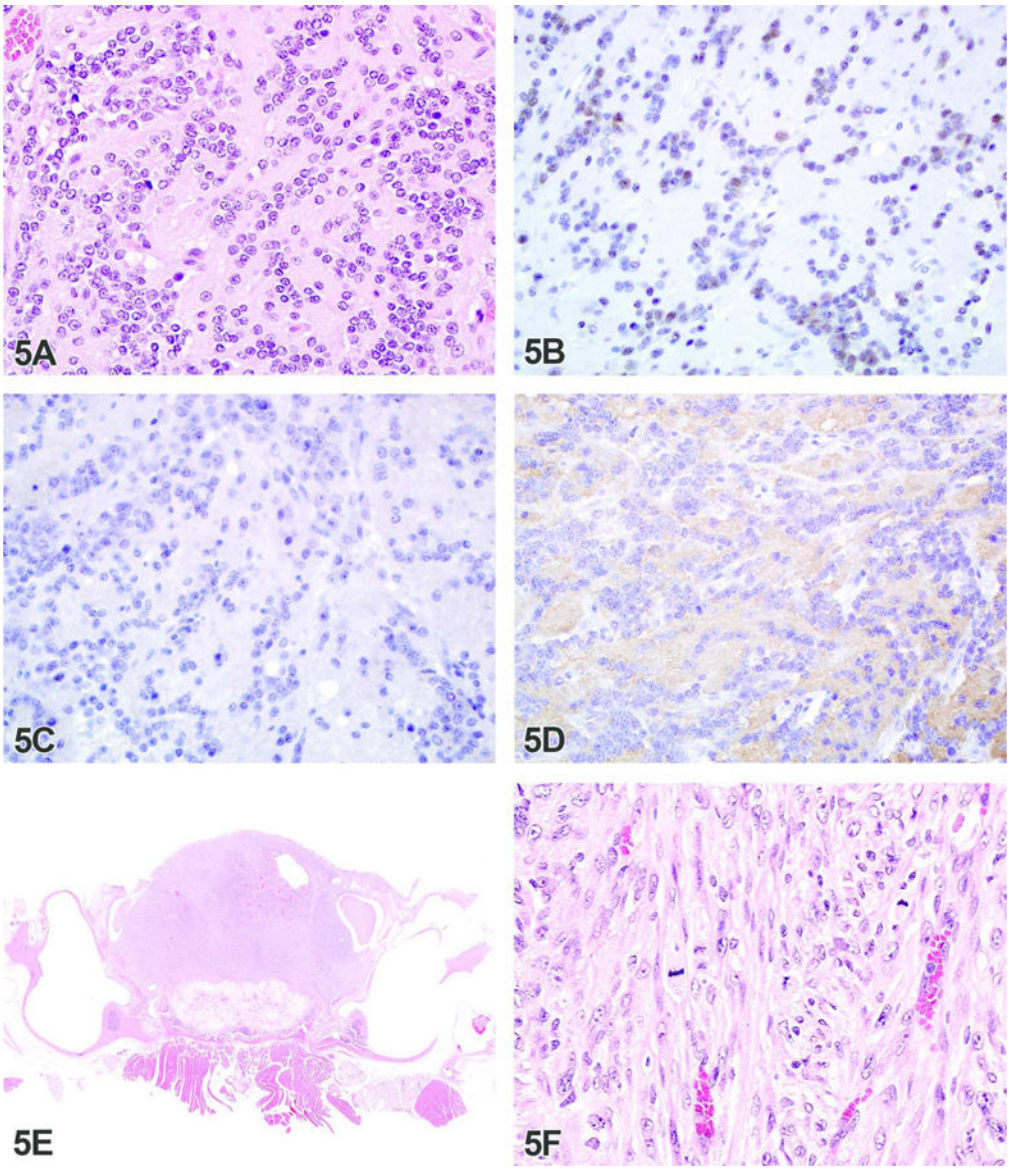

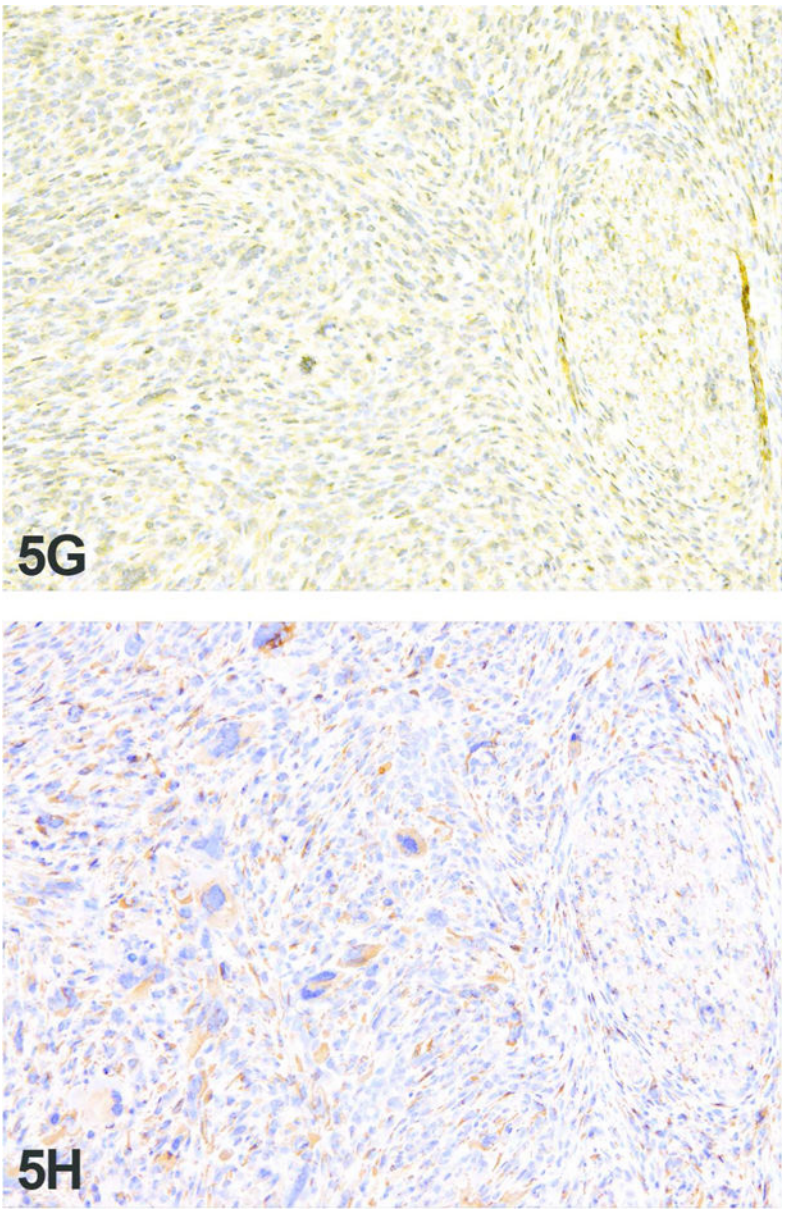

Figure 5.

(A–F). Two rare neoplasms in the rat brain. (A) High magnification, H&E image of a rat neurocytoma. Note the uniform neoplastic cells with small, round nuclei interspersed with eosinophilic fibrillary material. Anti-Neu N IHC (B); note the variably intense nuclear staining of the neoplastic cells. Anti-Olig2 IHC (C); the neoplastic cells are uniformly negative. Anti-synaptophysin IHC (D); the fibrillary material interspersed with the neoplastic cells is positive, consistent with the interpretation that this material represents the elaboration of cellular processes from the neoplastic cells. (E) Low magnification H&E image of a rat malignant pituicytoma. (F) High magnification H&E image demonstrating the spindle cell morphology, cellular pleomorphism and high mitotic rate.

(G–H). Anti-vimentin IHC (G); note the strongly positive cytoplasmic staining. Anti-GFAP IHC (H); note the strongly positive cytoplasmic staining. Images 5E, 5F, 5G and 5H were reproduced with permission from Moroki et al., 2015.

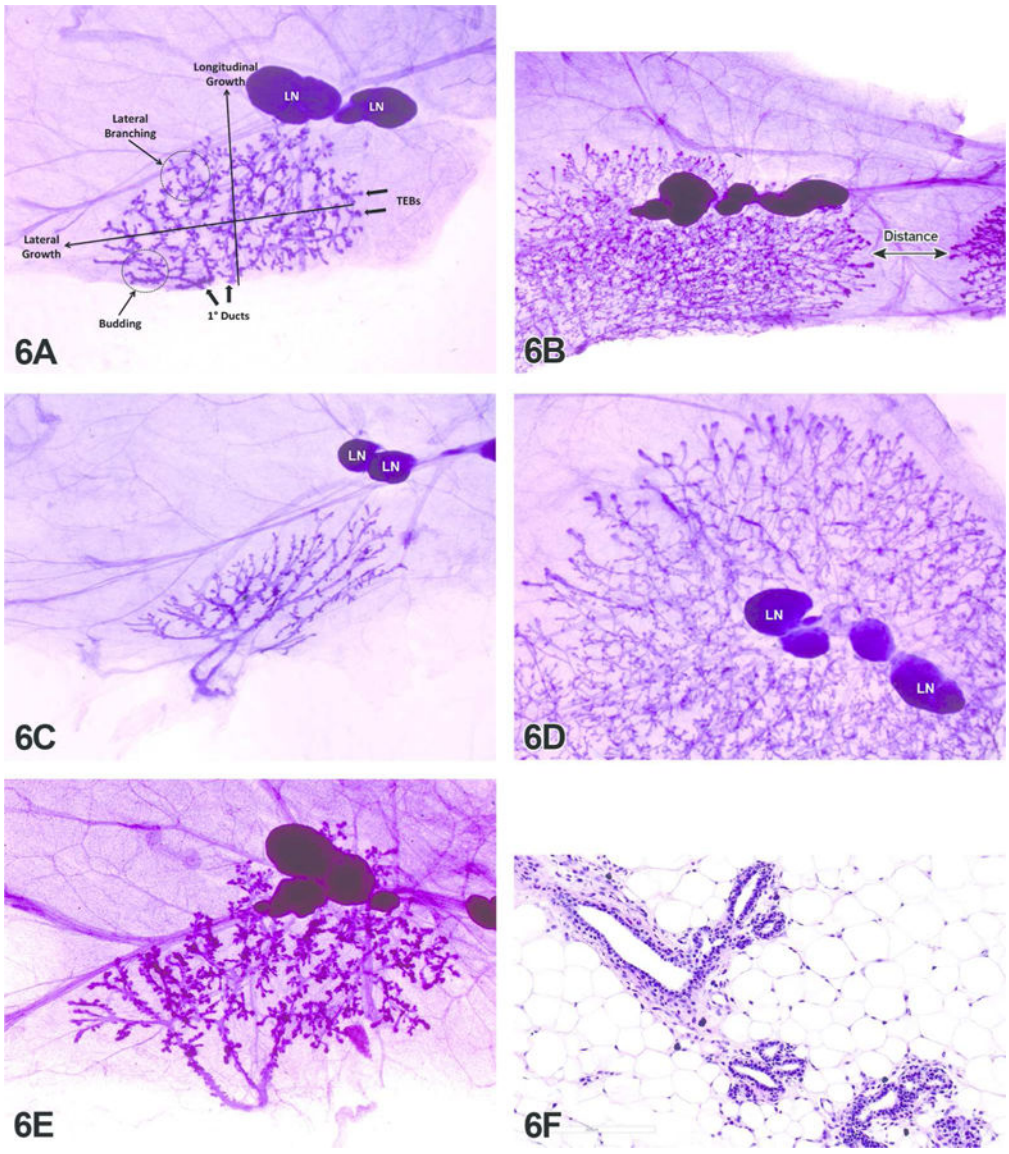

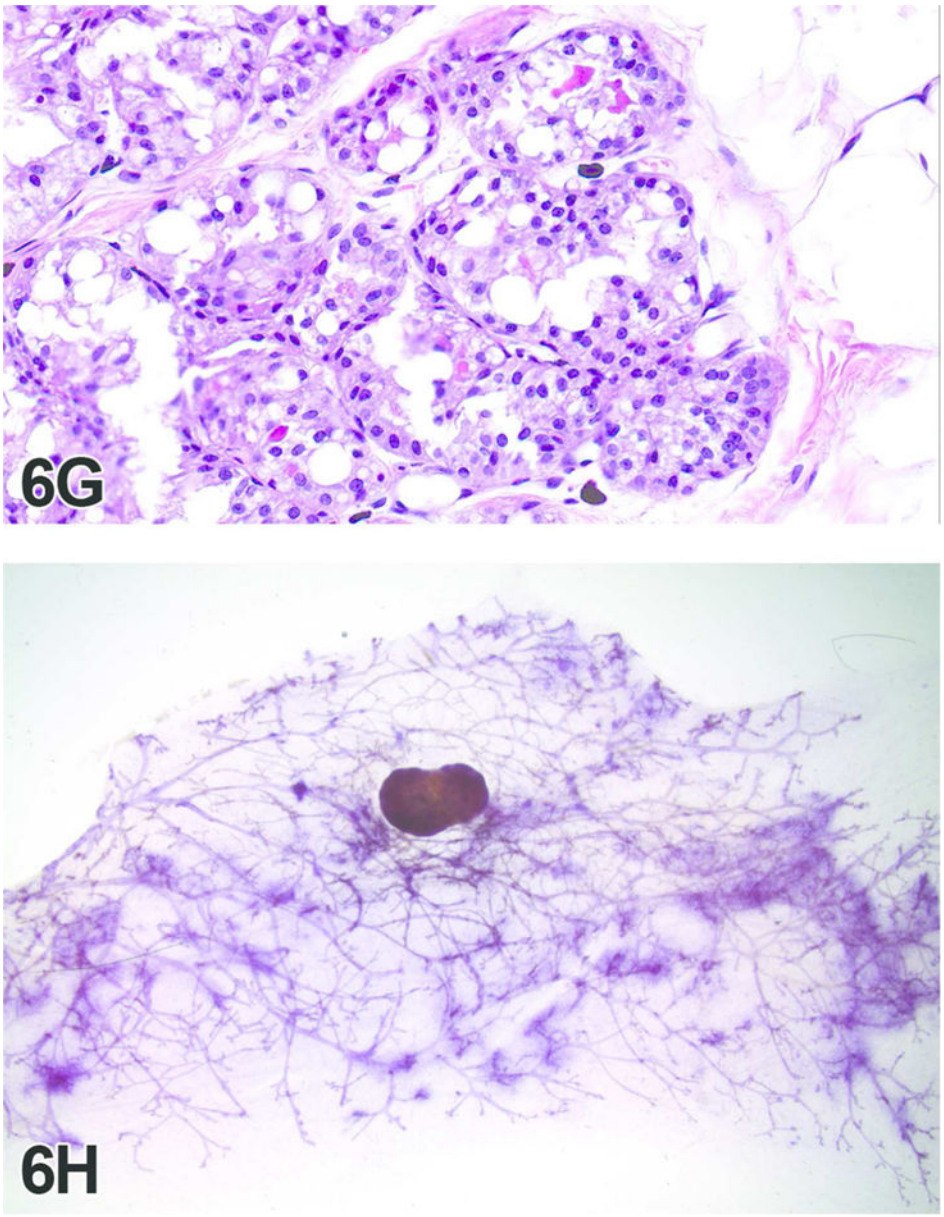

Figure 6.

(A–F). Examples of mammary gland whole mount preparations from treated and control rats and mice. (A) Mammary gland whole mount preparation, 21-day-old Sprague Dawley rat, female, control. Developmental scoring of the mammary gland is achieved by evaluating the indicated parameters: (1) lateral growth, (2) longitudinal growth, (3) the number of primary ducts arising from the nipple, (4) budding (branch density), (5) lateral (side) branching, and (6) the number of TEBs (carmine alum stain). (B) Mammary gland whole mount preparation, 33-day-old Sprague Dawley rat, female, prenatal exposure from gestation days (GD) 15–18, TCDD (2,3,7,8-tetrachlorodibenzo-*p*-dioxin). Distance between the 4th and 5th mammary glands are also assessed as these glands grow together in the maturing animal, eliminating the space between them (carmine alum stain). (C) Mammary gland whole mount preparation, 21-day-old Sprague Dawley rat, female, exposure from GD 6 to post-natal day

(PND) 90, 2.5mg/kg BPA (bisphenol A). Note markedly delayed development relative to age-matched control (Figure 6A) with decreased number of primary ducts and TEBs, decreased lateral and longitudinal growth, and decreased budding and lateral branching (carmine alum stain). (D) Mammary gland whole mount preparation, 21-day-old Sprague Dawley rat, female, exposure from GD 6 to post-natal day (PND) 90, 25 mg/kg EE_2 (ethinyl estradiol). Growth is markedly accelerated compared to the age-matched control (A). The gland is very dense, with many terminal end buds along the periphery and branching that extends well beyond the inguinal lymph node (carmine alum stain). (E) Mammary gland whole mount preparation, 21-day-old Sprague Dawley rat, female, control. The entire structure of the gland can be visualized via whole mount preparation, however cellular features are not observed (carmine alum stain). (F) Histology of the mammary gland, 21-day-old Sprague Dawley rat, female, control. The tubuloalveolar morphology of the female rat mammary gland is easily appreciated under light microscopy, yet the overall structure of the gland cannot be interpreted from this single section (H&E). LN= lymph node, TEB = terminal end buds.

(G–H). (G) Histology of the mammary gland, 21-day-old Sprague Dawley rat, male, prenatal exposure from GD 15–18 with DES (Diethylstilbestrol). The cellular morphology of the male rat mammary gland is typically lobuloalveolar in appearance. However, when exposed to estrogenic compounds such as DES during critical developmental time points, “feminization” of the gland may occur, causing the morphology to become more tubuloalveolar (inset) (H&E). (H) Mammary gland whole mount preparation, 14-month old, CD-1 mouse, female. Note the increased areas of opacity throughout the gland. These areas may indicate inflammation, hyperplasia or neoplasia. However, histological examination is required to confirm, as cellular features are not apparent (carmine alum stain).

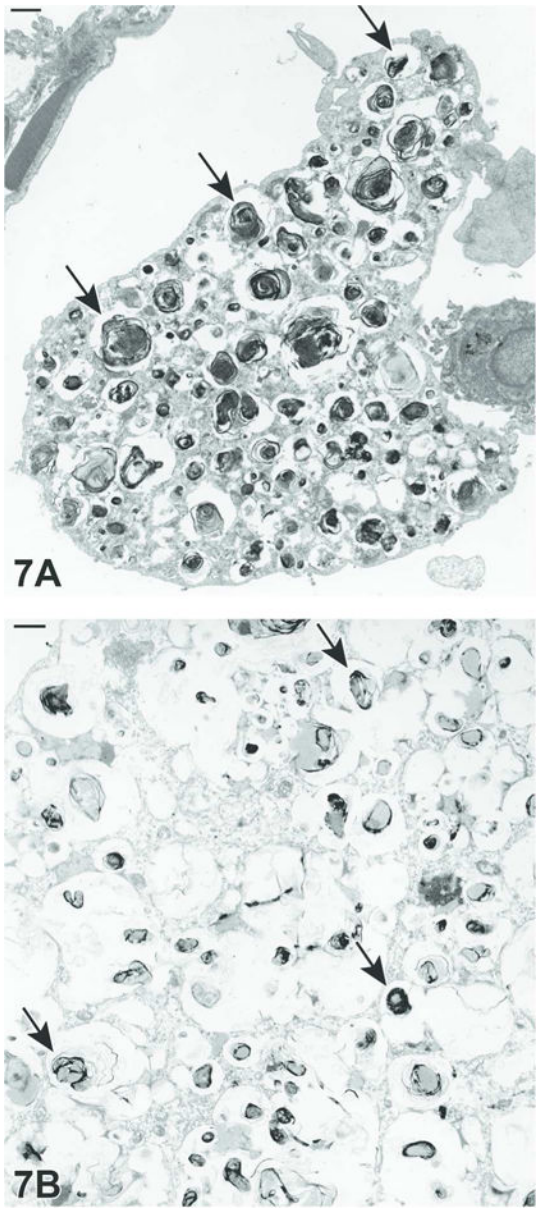

Figure 7.

(A–B). Transmission electron micrographs (TEMs) of rat and dog pulmonary pathologies. (A) TEM of an alveolar macrophage from a treated male rat lung that shows numerous secondary lysosomes (arrows) containing whorled membrane remnant material (Original micrograph magnification of 10,700×; Scale bar: 1 μM). (B) TEM of the cytoplasm of an alveolar macrophage from a treated female dog lung with numerous secondary lysosomes (arrows) containing whorled membrane remnant material with a central homogenous area (Original micrograph magnification of 10,700×; Scale bar: 1μM).

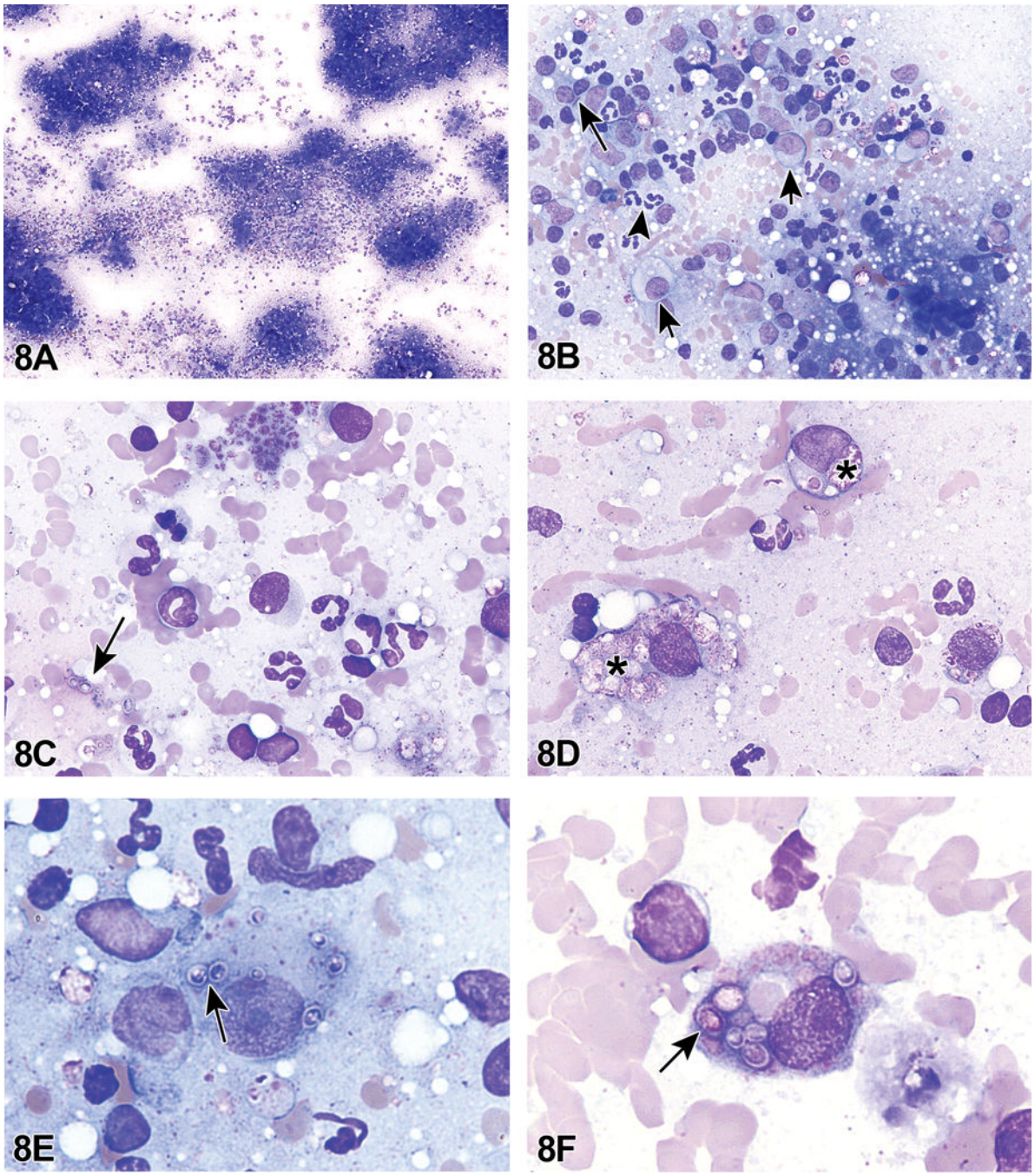

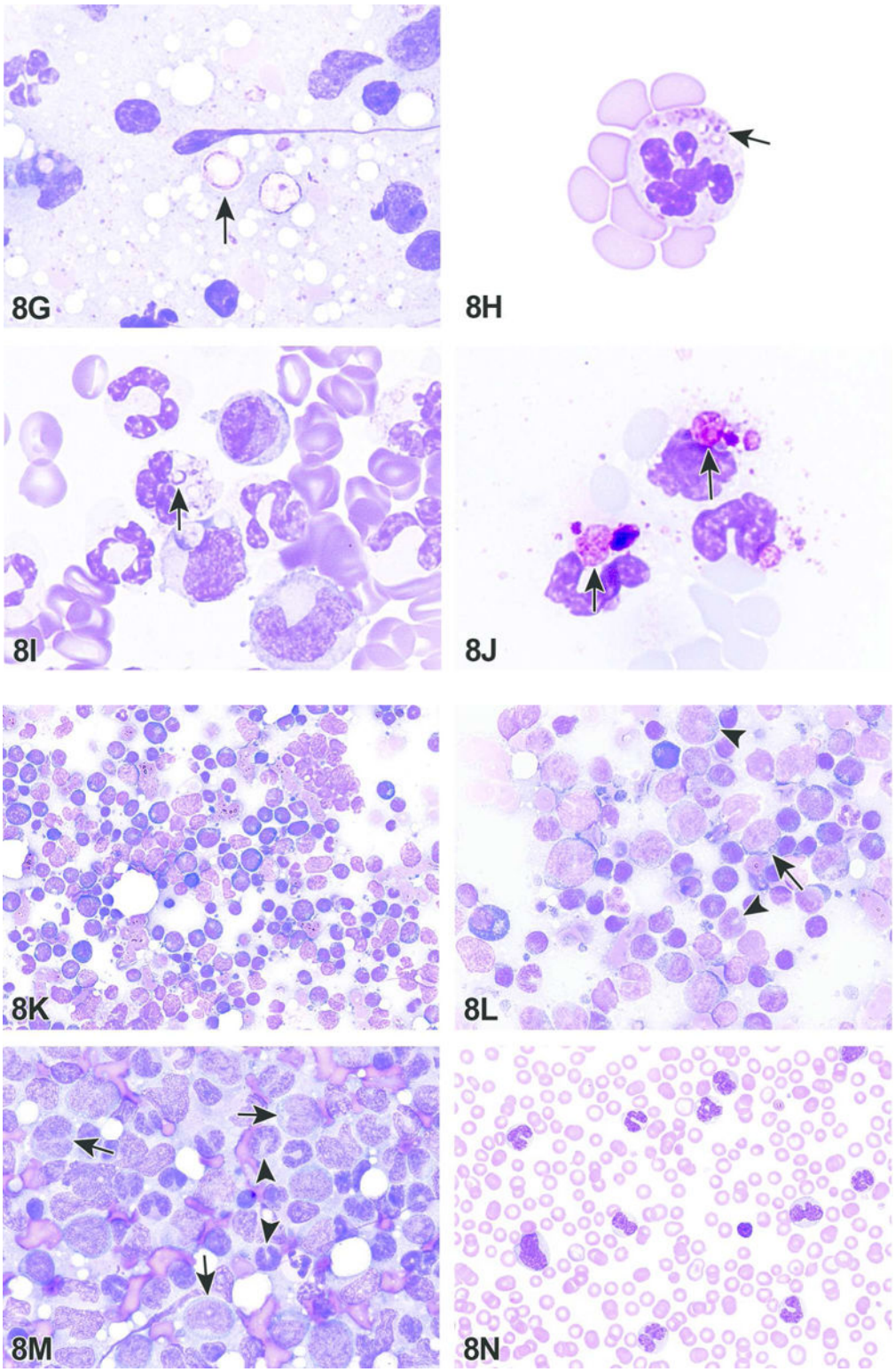

Figure 8.

(A–F). Liver aspirate from a cat with histoplasmosis. On low power, there is high cellularity with deeply basophilic clusters of hepatocytes and many cells in the background (A). Closer

examination of the background cells reveals a mixed inflammatory cell population consisting of neutrophils (arrowhead), histiocytes (short arrows) and lymphocytes (long arrow) (B). (C) While rare extracellular round yeast organisms with the classic appearance of *Histoplasma capsulatum* are seen (arrow, C), the more common finding consists of histiocytes with intracytoplasmic round stippled pink structures interpreted as degenerating organisms (asterisks, D). Rare macrophages with intact organisms (arrow) are also found (E), while rare partially degraded forms (arrows) are noted within cells (F). Wright-Giemsa stain.

(G–J). Rare partially degraded forms were also noted in the background (arrow, G). The appearance of the presumed degenerating organisms is not specific; items with a similar appearance include phagocytized and degraded mast cell granules (arrow, H), ragocytes with phagocytized immunoglobulin, fibrin and complement (arrow, I), or even phagocytized lubricant material (arrow, J), Wright-Giemsa stain.

(K–N). Lymph node aspirate from a dog with infiltrative chronic monocytic or myelomonocytic leukemia. On low power (K), there is a mixed round cell population. On higher power (L, M), many of the cells have band (arrowheads) to indented (short arrows) to irregularly-shaped (long arrow) nuclei with fine, dispersed chromatin indicating myeloid origin. An image of the peripheral blood smear (N) from this dog shows a similar population. However, the nuclear pleomorphism is more apparent, and the cells often contain a few vacuoles suggesting monocytic origin. Wright-Giemsa stain.

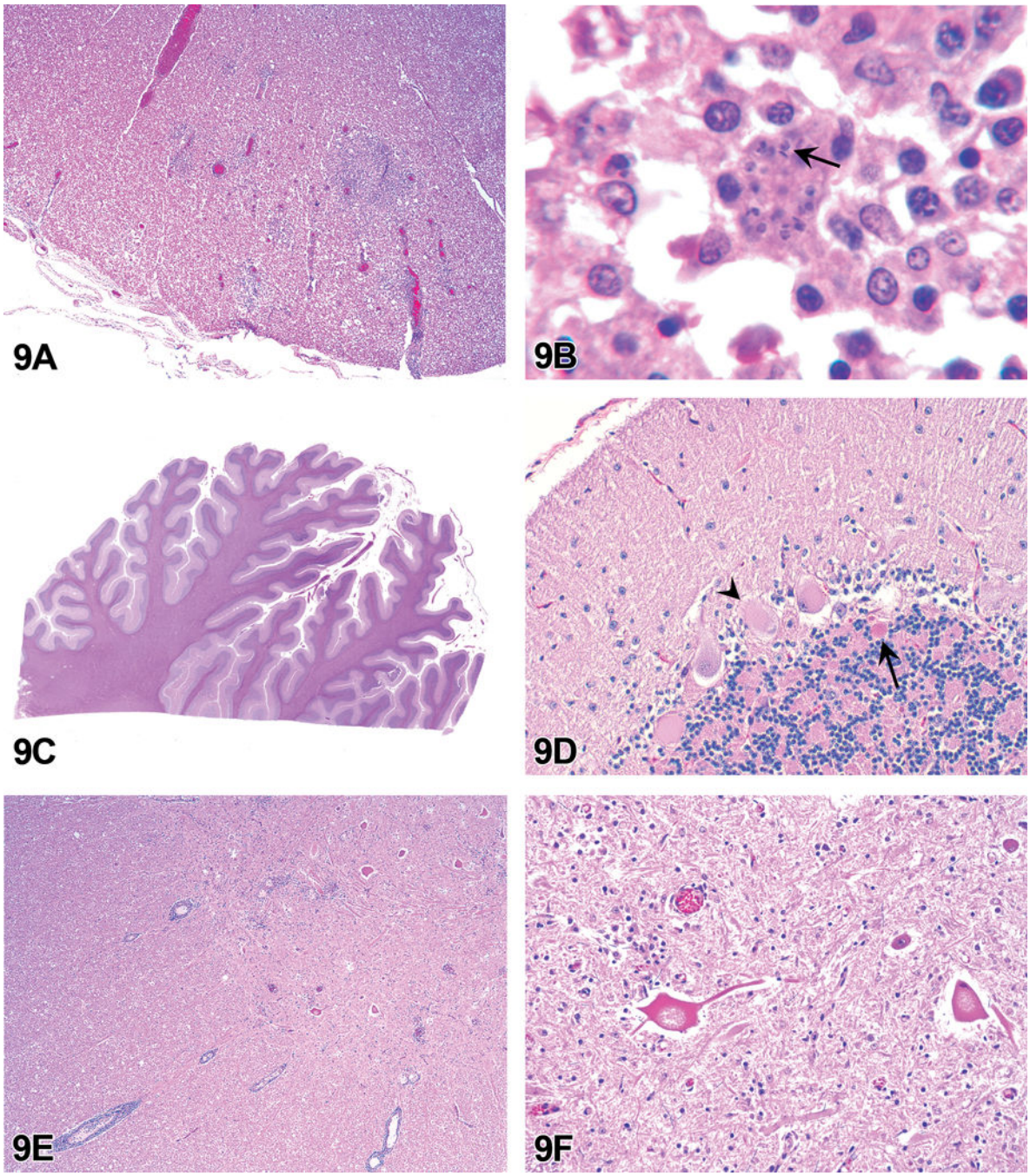

Figure 9.

(A–F). Chagas' disease in the spinal cord of a dog (A–B), *Solanum* toxicity in the cerebellum of a cow (C–D), and bovine astrovirus myelitis in a heifer (E–F). Multifocal inflammatory foci (A) are within the spinal cord white matter. Higher magnification (B) shows macrophages, lymphocytes, and plasma cells. The macrophage in the center contains protozoal amastigotes consistent with *Trypanosoma cruzi* (arrow). Subgross image of the cerebellum (C) shows thinning of the cerebellar folia. Higher magnification (D) shows swelling and vacuolation of Purkinje cells, loss of Purkinje cells with replacement by

proliferating Bergmann's glia, and a swollen Purkinje cell axon (arrow). Low magnification of the spinal cord (E) shows perivascular cuffing by lymphocytes and plasma cells, hypereosinophilic necrotic neurons, and gliosis. Higher magnification of the necrotic neurons and gliosis (F). The scattered bacteria are postmortem contaminants. (H&E)

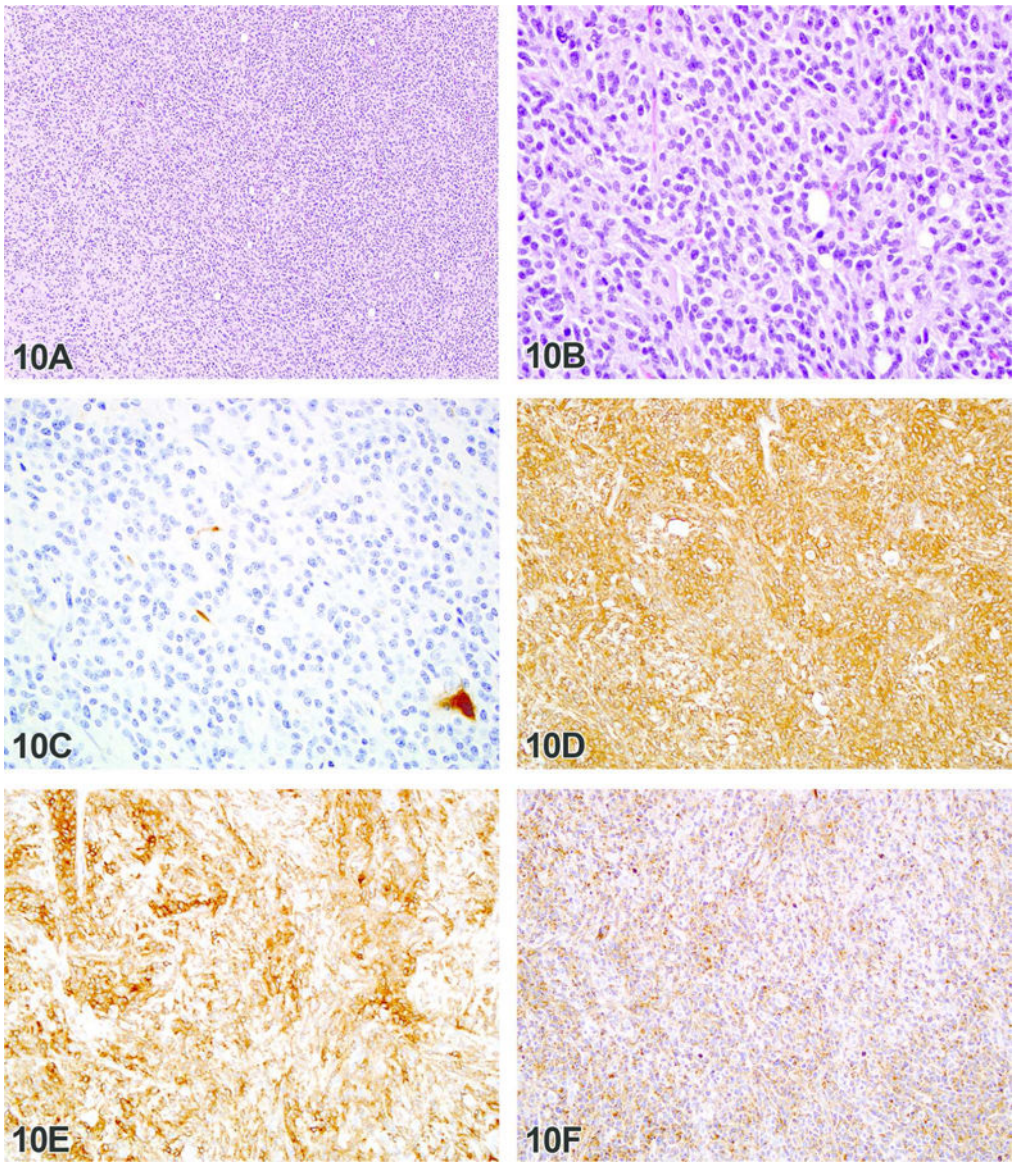

Figure 10.

(A–F). Intracranial neoplasm from a control male F344 rat. Low (A) and high (B) magnification, H&E images of what has historically been diagnosed as a rat astrocytoma. Note the lack of staining in the neoplastic cells with anti-GFAP immunohistochemistry (C). Note the diffuse positive staining for Iba-1 (D), MHC Class II (E) and by the plant lectin RCA-1 (F). The above results support a microglial or macrophage rather than an astrocytic histogenesis.

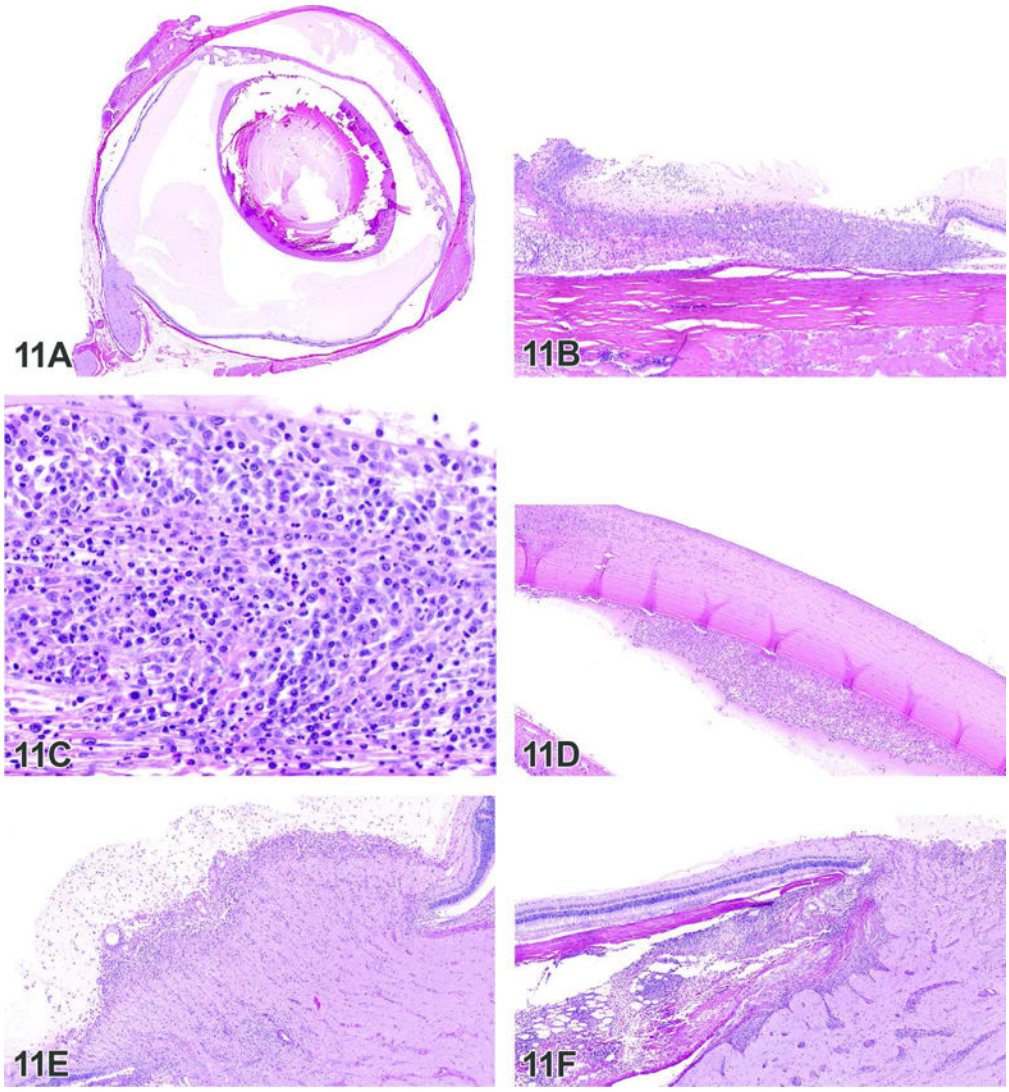

Figure 11.

(A–F). Lesions from a 14-day single-dose ITV administration study in New Zealand White rabbits. (A) Overview of the eye, showing eosinophilic, amorphous material in the anterior and posterior compartments, compatible with proteinaceous fluid. Mixed cell inflammation in the pars planum (B) and a higher power view (C) of the inflammation, showing a mixture of mononuclear cells, including plasma cells, and heterophils. There is mixed cell inflammation in the anterior chamber, aligning the endothelial surface of the cornea, as well as inflammation within the corneal stroma (D), mixed cell inflammation in the optic nerve head and in the adjacent vitreous (E) and mixed cell inflammation within the optic nerve, as well as external to the eye surrounding the optic nerve (F). H&E.

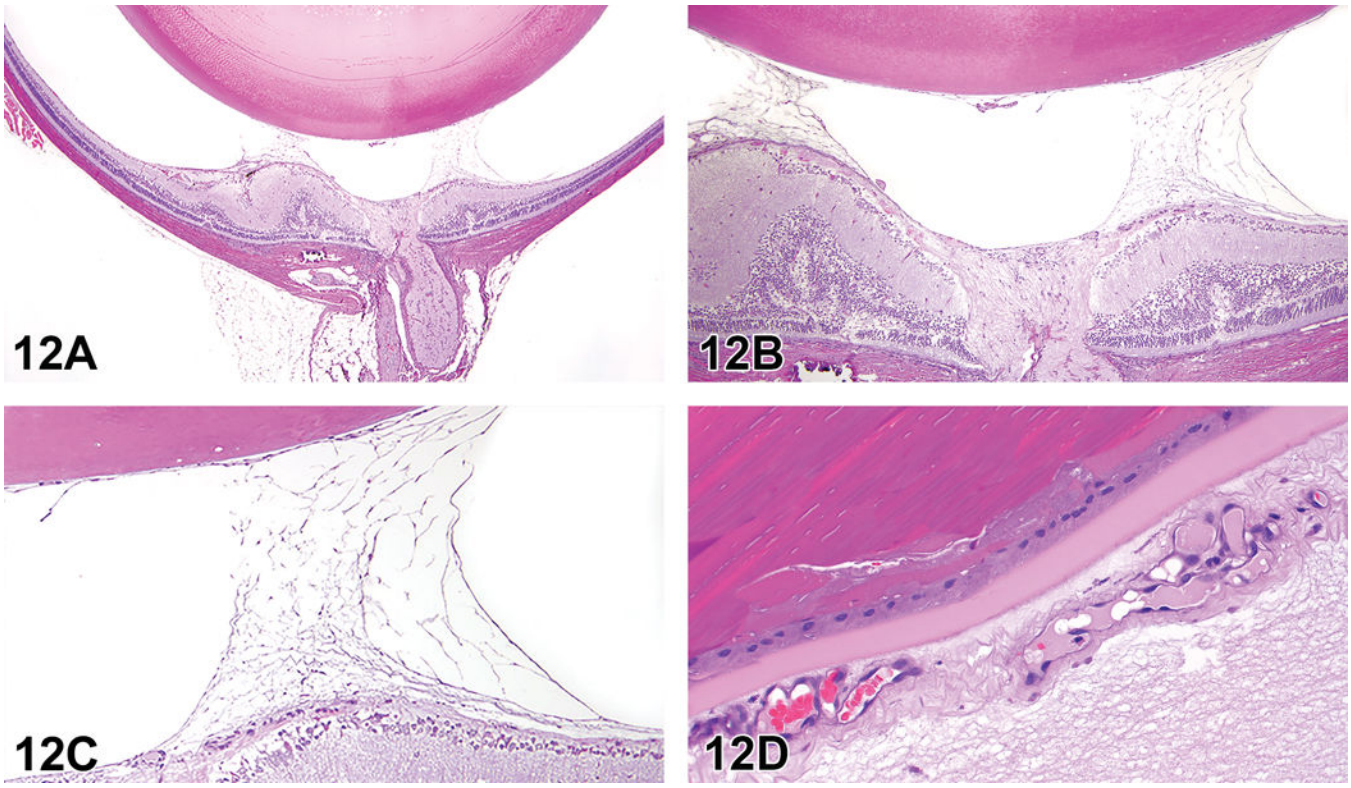

Figure 12.

(A–D). Eye of a Sprague-Dawley rat. Low magnification image (A) showing the optic nerve and central retina. There is a delicate fibrovascular tissue extending from the surface of the retina into the vitreous, contacting the posterior lens capsule. Higher magnifications (B & C), showing the fibrovascular nature of the tissue causing retinal traction and folds. Anterior portion of the tissue (D) consistent with a persistent hyperplastic tunica vasculosa lentis (PHTVL) characterized by small and regularly distributed vessels surrounding the posterior lens capsule. H&E.

Table 1

Summary of Voting Options and Results for Heart Lesions

Voting Percentage (%)							
		Case 1	**Case 2**	**Case 3**	**Case 4**	**Case 5**	**Case 6**
Voting Options	Inflammatory cell infiltrate	3	67	11	13	27	42
	Necrosis	11	1	1	0	0	2
	Fibrosis	1	0	0	0	0	0
	Inflammatory cell infiltrate and necrosis	13	4	9	6	0	0
	Inflammatory cell infiltrate and fibrosis	1	1	2	3	NA	NA
	Inflammatory cell infiltrate and necrosis and fibrosis	2	0	2	5	NA	NA
	Degeneration/necrosis	27	0	8	5	1	0
	Necrosis/inflammatory cell infiltrate (NICI)	23	17	39	37	4	7
	Cardiomyopathy	20	10	26	31	1	5
	Not a lesion or equivocal	NA	NA	NA	NA	44	14
	Definite lesion, but below my threshold for diagnosis	NA	NA	NA	NA	22	30
	Minimal	NA	38	54	29	NA	NA
	Mild	NA	37	37	53	NA	NA
	Moderate	NA	19	8	18	NA	NA
	Severe	NA	6	1	1	NA	NA

NA-not applicable

Table 2

Gross Composition (%) of Milk from Various Avian and Mammalian Species*

	Fat	Protein	Carbohydrate (Lactose)	Ash	Total Solids
Pigeon	10	23	0		33.0
Penguin	29	59	5.5		93.5
Flamingo	18	8	0.2		26.2
Rat	14.8	11.3	2.9	1.5	31.8
Rabbit	12.2	10.4	1.8	2.0	26.4
Human	4.5	1.1	6.8	0.2	12.6
Seal	53.2	11.2	2.6	0.7	67.7
Whale	34.8	13.6	1.8	1.6	51.2

* Data are from previously published studies (Schmidt-Nielsen, 1979; Park and Haenlein, 2006)

Table 3

Lung and Pancreatic Proliferative Lesions in Male F-344 Rats given (*S*)-NNAL, (*R*)-NNAL, NNK, or Racemic NNAL in Drinking Water*

	Control	(*R*)-NNAL 5 ppm	(*S*)-NNAL 5 ppm	NNK 5 ppm	Racemic NNAL 10 ppm
No. of rats necropsied	22	24	22	24	15
No. of rats with lung lesions					
Hyperplasia	0	24	22	24	15
Adenoma	0	23	22	24	15
Carcinoma	0	6[a]	10[a]	17[a]	15[a]
Tumor Incidence	0	23[b]	22[b]	24[b]	15[b]
No. of rats with thoracic cavity tumors	0	2	2	6	9
No. of rats with metastasis to pancreas	0	1 (4.2%)	2 (9.0%)	3(12.5%)	4[c] (27.0%)

[a] P <0.01 compared to control

[b] P <0.0001 compared to control

[c] P<0.05 compared to control (ψ^2 test)

* Reproduced with modifications from Balbo et al., 2014